Det Kongelige Danske Videnskabernes Selskab
Matematisk-fysiske Meddelelser, bind **29**, nr. 15

Dan. Mat. Fys. Medd. **29**, no. 15 (1955)

CONSTRUCTION OF A SPECTROMETER FOR NEUTRINO RECOILS: INVESTIGATION OF THE DECAY OF A^{37}

BY

O. KOFOED-HANSEN AND A. NIELSEN

København 1955
i kommission hos Ejnar Munksgaard

CONTENTS

Printed in Denmark.
Bianco Lunos Bogtrykkeri A-S.

A neutrino recoil spectrometer has been constructed. The motion of the recoils has been studied in crossed electric and magnetic fields. The particles have been detected by the charge they give off to the collector system.

First, the theory of the instrument is described; subsequently, details of its construction are given and, finally, results obtained in an investigation of A^{37} are presented. These results are:

The neutrino momentum 812 ± 8 keV
pct. recoils of charge 1 26 ± 3
pct. recoils of charge 2 13 ± 4
pct. recoils of charge 3 38 ± 4
pct. recoils of charge 4 18 ± 2
pct. recoils of charge 5 4 ± 1
pct. recoils of charge 6 1 ± 1

The average charge of the charged recoils $2.64 \pm .08$.
Momentum of the most energetic Auger electrons 162 ± 4 Gauss cm.
pct. of decays leading to such electrons 65 ± 5.
Average momentum of all electrons 69 ± 1 Gauss cm.

Introduction.

Neutrino recoil particles have in general energies of the order of a few electron volts. The most reliable investigations of such recoils can therefore be carried out with radioactive noble gases. In such experiments, no disturbing effects from source backing or molecular break-up appear.

Ordinarily, it is tried to measure neutrino recoils in instruments which are similar to conventional spectrometers. A radioactive noble gas, however, inevitably spreads out over the whole volume of the chamber. This introduces complications in the evaluation of the resolution curves for the instrument.

In the present article, an instrument is described which has very few similarities to conventional spectrometers. The purpose of this change is to obtain an instrument of sufficient simplicity so that it is feasible to carry through a complete mathematical

analysis of the factors determining intensity and motion of the particles.

We shall study the orbits of the recoils in homogeneous electric and magnetic fields produced inside the volume of a plane parallel condenser. Further, the motion of the particles will be investigated by measuring the charges they give off when they hit the plates of the condenser. The mathematical problem arising is then simply the question of whether a given particle produced in a given position, with a given charge to mass ratio and velocity, will hit a certain one of the condenser plates, or whether it will spiral out between the plates. We then choose such values of the fields which permit the separation of the effects from the different particles. The measuring procedure involves studying small variations in the currents when the fields are changed in such a manner that these changes can be interpreted with respect to the kinematic parameters describing the particles.

With the present choice of the geometry of the instrument, it will be our task to measure currents from particles starting everywhere inside the condenser and with all directions of initial velocity. This obviously leads to many integrations, a fact which makes it evident that we are dealing with very poor geometry. At first sight, it might appear as if the worst possible geometry had been chosen; this suspicion can only be disproved by our results which have provided a body of information that so far had not been obtained by means of more conventional types of spectrometers.

In the following, we shall first enter into the theory of the instrument by solving the mathematical program formulated above. Then, the construction of the instrument is described and an analysis of some necessary measurements is given, which have been carried out in order to determine the behaviour of the instrument. Finally, the results obtained in an investigation of the recoils from K-capture of A^{37} are presented.

Chapter 1. Theory of the Instrument.

1.1 Principle of the Instrument.

In principle, the chamber of the instrument consists of an evacuated space between two condenser plates (Fig. 1). An electric voltage V is applied across the condenser. A magnetic

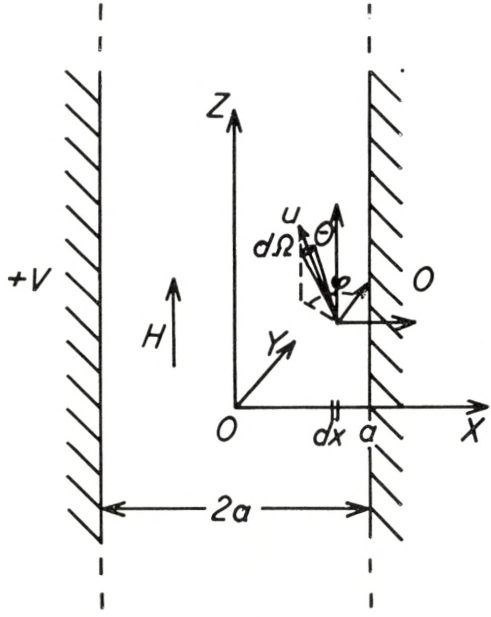

Fig. 1. Principle of the instrument.

field H is introduced parallel to the plane of the condenser plates and a radioactive noble gas is introduced into the space between the plates. When the gas decays, charged particles are created uniformly throughout the space between the plates and with no preferred direction of emission relative to the orientation of the electric and magnetic fields. By β-decay charged recoils appear. Furthermore, secondary effects, such as Auger transitions and influence of nuclear charge changes, give rise to secondary electrons. Thereby high charge values on the recoil atoms may be obtained. In the following, we therefore consider an initially

homogeneously distributed creation of recoil particles with the ionic charge spectrum n_{z_γ} and momentum distribution $P(Mu)$ together with electrons of momentum distribution $P(p)$. The number of recoils created per second inside the interval between x and $x + dx$ (cf. Fig. 1), and with direction of emission inside the solid angle $d\Omega = (1/4\,\pi)\,\sin\theta\,d\theta\,d\varphi$ with charge z_γ and momentum between Mu and $Mu + dMu$, is consequently assumed to be given by

$$N n_{z_\gamma} P(Mu)\,dMu\,(dx/2\,a)\,(1/4\,\pi)\,\sin\theta\,d\theta\,d\varphi\,, \tag{1}$$

where N is the total number of disintegrations per second, and $2\,a$ is the distance between the condenser plates (cf. Fig. 1). Similarly, the number of electrons created per second between x and $x + dx$, and with momentum between p and $p + dp$, and with the direction of emission inside the solid angle interval $d\Omega$, is given by

$$N\langle z_\gamma\rangle\,P(p)\,dp\,(dx/2\,a)\,(1/4\,\pi)\,\sin\theta\,d\theta\,d\varphi\,, \tag{2}$$

where $\langle z_\gamma\rangle$ is the average charge of the recoils. Since we start with neutral atoms, charge conservation tells us that in all $N\langle z_\gamma\rangle$ electrons have to be accounted for. This number of electrons of course includes the decay electrons when we are dealing with a β^--decay. In the case of β^--decay including e emission to a bound state, K-capture, and isomeric transitions, only neutral or positively charged recoils appear. We shall restrict our considerations to such cases, although the theory of the instrument, with slight extensions, can also be applied to β^+-decay.

When charged particles move in crossed electric and magnetic fields, the orbits are determined essentially by the velocity and the charge to mass ratio. Thereby the different contributions to n_z, $P(Mu)$, and $P(p)$ can be found by studying the motion of the particles at different values of the field strengths $F = V/2\,a$ and H. As mentioned in the Introduction, the variations of the orbits are studied by following the variation of the numbers of particles hitting the plates of the condenser. This number can be examined in essentially two different ways. The number of particles has previously been measured by the tracer method[1] and only electric fields have been applied. In the present investigation,

the particles are detected by the charge they give off to the plates. In cases where the tracer method can be used, both neutral and charged recoils are detected and, furthermore, no contribution from the electrons has to be considered. Such cases appear when the radioactive noble gas has a radioactive daughter substance. When currents are measured, the electrons have also to be taken into account. The large difference between the charge to mass ratio for recoils and that for electrons is the most important factor used in distinguishing between the contribution from each of these types of particles. This difference causes great changes in the orbits of the light and heavy particles. The motion of the electrons is essentially determined by the magnetic fields, and the introduction of small electric fields causes only very small corrections. Conversely, for the recoils the electric fields are of greatest importance.

When currents are measured, neutral particles do not contribute. Thus, in the following, we have to interpret the number N as the number of decays leading to charged particles and our discussions refer to the charged decay products only. In formulas (1) and (2), we have therefore also assumed the following normalization condition

$$\sum_{z_\gamma = 1}^{\infty} n_{z_\gamma} = 1 . \tag{3}$$

For completeness, it should be mentioned that the momentum spectra are also assumed to be normalized in the following way:

$$\int_0^\infty P(p)\, dp = 1 , \tag{4}$$

$$\int_0^\infty P(Mu)\, dMu = 1 . \tag{5}$$

In order to illustrate the procedure of calculating the currents as functions of V and H, we begin with the very simple example which occurs when $Mu = 0$. Such calculations are very illustrative of the procedure adopted in the following, and the results constitute an important limiting case for our later calculations which take into account the momentum of the particles.

1.2 Particles Initially at Rest.

In order to facilitate the understanding of the instrument, we separate the two problems, charge distribution and momentum distribution and, in this section, discuss particles initially at rest. The equations of motion (cf. eq. 33, ref. 2) in the non-relativistic limit are

$$M\ddot{x} = z_\gamma eF + (z_\gamma e/c)\, H\dot{y}, \tag{6}$$

$$M\ddot{y} = -(z_\gamma e/c)\, H\dot{x}, \tag{7}$$

$$M\ddot{z} = 0. \tag{8}$$

With the conditions $\dot{x}(t = 0) = 0$, we get the well-known cycloidal orbits of the motion

$$x - x_0 = (Mc^2F/z_\gamma eH^2)\,[1 - \cos(z_\gamma eH/Mc)\,t], \tag{9}$$

$$y - y_0 = (Mc^2F/z_\gamma eH^2)\sin(z_\gamma eH/Mc)\,t - (F/H)\,ct, \tag{10}$$

$$z - z_0 = 0. \tag{11}$$

The motion is a plane motion. It should also be noted that, in (9)—(11), the kinematic parameters and the fields enter through the combinations

$$aB_{z_\gamma} = (Mc^2F/z_\gamma eH^2), \tag{12}$$

$$D = cF/H \tag{13}$$

only.

Due to the periodicity of the orbits as regards the motion in the x-direction, we can obtain an experimental approach to an infinitely extended condenser system by introducing a central collector plate (cf. Figs. 8 and 9 of ref. 2) and the necessary guard rings or protection plates. The necessary sizes of the guard rings are discussed in ref. 2 for the cases of pure magnetic and electric fields. The guard ring discussion in crossed electric and magnetic fields proceeds essentially along the same lines and no further details will be given here. We may only mention that the instrument actually was constructed in such a way as to make it most suitable for our purposes.

We can then proceed as if the condenser were infinitely extended in the y- and x-directions. In order to discuss the number of particles hitting the plates, it is therefore necessary to examine the magnitudes $x^{\max}$ and $x^{\min}$ only. Since, in this special case of the initial velocity $u = 0$, we have

$$x^{\min} = x_0, \tag{14}$$

we are even satisfied when we know the amplitude of the motion in the x-direction, i. e.,

$$x^{\max} - x^{\min} = (2\, Mc^2 F / z_\gamma e H^2) = 2\, a\, B_{z_\gamma}. \tag{15}$$

From this information we find immediately the relative number of particles hitting the positive plate

$$h(B) = 0. \tag{16}$$

The number of particles moving out towards infinity is given by

$$g(B) = \begin{cases} 1 - \dfrac{x^{\max} - x^{\min}}{2\, a} \\ 0 \end{cases} = \begin{cases} 1 - B \text{ for } B < 1 \\ 0 \quad \text{for } B > 1 \end{cases} \tag{17}$$

and the number of particles hitting the negative plate is given by

$$f(B) = \begin{cases} \dfrac{x^{\max} - x^{\min}}{2\, a} \\ 1 \end{cases} = \begin{cases} B \quad \text{for} \quad B < 1 \\ 1 \quad \text{for} \quad B > 1. \end{cases} \tag{18}$$

It is obvious that the functions h, g, and f fulfill the condition

$$h(B) + g(B) + f(B) = 1. \tag{19}$$

The currents obtained for a certain charge distribuion n_{z_γ} are correspondingly given by

$$\left.\begin{matrix} i_+ \\ i_{\text{out}} \\ i_- \end{matrix}\right\} = eN \sum_{z_\gamma} z_\gamma n_{z_\gamma} \left\{\begin{matrix} h(B) \\ g(B) \\ f(B) \end{matrix}\right. \tag{20}$$

and, according to (19), the currents fulfill

$$i_{\text{out}} = eN\langle z_\gamma \rangle - i_+ - i_-. \tag{21}$$

In order to get an idea of the accuracy which can be obtained in a determination of n_{z_γ} from measured currents, imagine that i_- has been measured for F equal to integral multiples of (eH^2a/Mc^2). Furthermore, let us denote the corresponding i_- values by i_1, i_2, i_3, etc. From (20) it is then seen that the results must be interpreted as

$$\left.\begin{aligned} n_1 + n_2 + n_3 + n_4 + \ldots\ldots\ldots &= i_1/N \\ n_1 + 2\,n_2 + 2\,n_3 + 2\,n_4 + \ldots\ldots &= i_2/N \\ n_1 + 2\,n_2 + 3\,n_3 + 3\,n_4 + \ldots\ldots &= i_3/N \\ n_1 + 2\,n_2 + 3\,n_3 + 4\,n_4 + \ldots\ldots &= i_4/N \end{aligned}\right\} \tag{22}$$

with the solutions

$$\left.\begin{aligned} Nn_1 &= 2\,i_1 - i_2 \\ Nn_{z_\gamma} &= 2\,i_{z_\gamma} - i_{z_\gamma - 1} - i_{z_\gamma + 1}, \end{aligned}\right\} \tag{23}$$

which indicates that a considerable accuracy can be obtained. When, initially, the particles have a distribution in velocity, the set of equations analogous to (22) is more complicated and the accuracy with which n_{z_γ} can be obtained is reduced.

Although we have omitted the initial velocity u in this discussion, all the essential features of the method with respect to a study of the charge distribution of the recoils are given in this section. Especially when $D \gg u$, all the details of i_+, i_-, and i_{out} are given by (20) to the second order in u/D.

Also the method which we apply for the calculation of h, g, and f as functions of B_{z_γ} and u is essentially similar to those outlined here. The important magnitudes are $x^{\max}$ and $x^{\min}$, and we have to separate the number of particles into those hitting the positive plate, those hitting the negative plate, and those spiralling out.

1.3 Particles with Finite Initial Velocity.

For the discussion of an infinitely extended condenser we first show that the motion is periodic in the x-direction. This has been done in ref. 2. Also $x^{\max}$ and $x^{\min}$ have been found in ref. 2. For a discussion of the motion of the heavy particles we take the non-relativistic approximation eq. (40) of ref. 2

$$\overset{\max}{x^{\min}} - x_0 = aB(1 + A'_y \pm [1 + 2A'_y + A'^2]^{1/2}) = \begin{Bmatrix} \omega a \\ -Wa \end{Bmatrix} \quad (24)$$

where we have introduced

$$A' = [u_x^2 + u_y^2]^{1/2}/D, \quad (25)$$

$$A'_x = u_x/D, \quad (26)$$

$$A'_y = u_y/D. \quad (27)$$

We shall also write

$$A = [u_x^2 + u_y^2 + u_z^2]^{1/2}/D, \quad (28)$$

where

$$\vec{u} = (u_x, u_y, u_z) = (-u \sin\theta \sin\varphi, u \sin\theta \cos\varphi, u \cos\theta). \quad (29)$$

The initial situation is illustrated in Fig. 1. We now introduce the relative numbers f, g, and h as in the preceding section. In order to calculate these numbers we introduce the dimensionless quantities W and ω defined in (24). It is seen that, after averaging over all directions in u, we find that the numbers f, g, and h are functions of A and B only, and that no other combination of the kinematic parameters and the fields appear in our formulas.

In Appendix A, which contains the results of some of the numerical calculations which have to be performed, a picture of the A—B plane is also given. In the present paper, we restrict ourselves to certain regions in this plane where the calculations are especially simple. The procedure will be to compare the quantities W and ω and the relative amplitude of the motion

$$L = W + \omega \quad (30)$$

to 2.

Region I in the A—B plane. The simplest case for our calculations is obtained when

$$\left.\begin{array}{r} L \geqslant 2 \\ \text{and} \\ W \leqslant 2 \end{array}\right\} \text{ i. e. } \left\{\begin{array}{l} B \geqslant 1/(1-A);\ A < 1;\ B < 3 + \sqrt{8} \\ \\ B \leqslant 4/A^2;\ A < 1;\ B > 3 + \sqrt{8}, \end{array}\right\} \tag{31}$$

independent of θ and φ. This case has been treated in detail in ref. 2, together with the simple cases in which we have a pure magnetic field and in which we have a pure electric field. This calculation can also be obtained as a special case of the following more general considerations.

Region II in the A—B plane. Another relatively simple calculation occurs when

$$L < 2, \quad \text{i. e.} \quad B < 1/(1+A), \tag{32}$$

independent of θ and φ. Both these cases are simple because we can freely integrate over the angles. There is, however, no reason for setting up special derivations for these regions; rather, we prefer to cover the entire region where

$$W \leqslant 2,$$

i. e.

$$\left.\begin{array}{ll} B \leqslant 1/(A-1) & \text{for } A \geqslant 2, \\ B \leqslant 4/A^2 & \text{for } 0 \leqslant A \leqslant 2. \end{array}\right\} \tag{33}$$

Physically, this means that the electric potential V is so large that particles starting out towards the positive plate from the immediate vicinity of the negative plate can never reach, or else can just touch, the positive plate. In the interval $0 \leqslant A \leqslant 2$ in (33), the condition is, as seen, $B \leqslant 4/A^2$ which leads to

$$V \geqslant T_R, \tag{34}$$

where T_R is the kinetic energy $\frac{1}{2} M u^2$ of the recoils. Under the restriction (33), we find that ω and W always roughly behave as indicated in Fig. 2 in the special case of $A' = B = 1$.

We have to divide our considerations into two parts according to the magnitude of φ. In each case, we can first estimate the

number of particles hitting the plate towards which it starts to move. Those which miss this plate have then to be separated into those that hit the other plate and those that spiral out, as shown in Fig. 2.

In order to integrate our expressions, we have of course to find the value of φ giving $L = 2$; if no such value exists, the

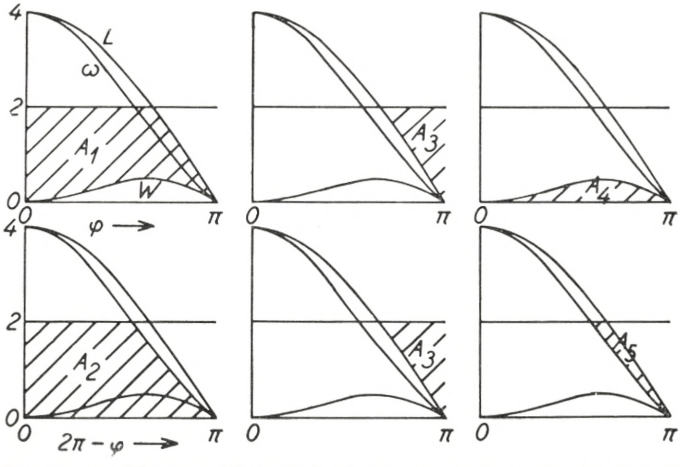

Fig. 2. The curves $W(\varphi)$, $\omega(\varphi)$, and $L(\varphi)$ are drawn for a fixed value of $A' = 1$ and $B = 1$. The number of particles is divided into two parts according to whether they start out towards the negative plate, i.e., $0 \leqslant \varphi \leqslant \pi$, or whether they start out towards the positive plate $\pi \leqslant \varphi \leqslant 2\pi$. In this way, it is easily seen that the contribution to f is given by $\frac{1}{2}(A_1 + A_2)$, the contribution to g is given by A_3, and the contribution to h is given by $\frac{1}{2}(A_4 + A_5)$, where the A_i's are the hatched areas shown in the figures.

limits of integration should be chosen as 0 or π. Thus, the limit of integration is

$$\varphi' = \left\{ \begin{array}{l} 0 \text{ for } B < 1/(1 + A') \\ \text{Arccos}\left[\frac{1}{2A'}\left(\frac{1}{B^2} - 1 - A'^2\right)\right] \text{ for } 1/(1 + A') < B < 1/(1 - A') \\ \pi \text{ for } B > 1/(1 - A'). \end{array} \right\} \quad (35)$$

Similarly, we have to find the value of φ giving $\omega = 2$. Corresponding to (35), we find

(48)

$$\varphi'' = \left\{ \begin{array}{l} 0 \quad \text{for} \quad B < 1/(1+A') \\ \text{Arccos}\,[2/BA' - [(4/BA'^2)+1]^{1/2}] \text{ for } 1/(1+A') < B < 1/(1-A') \\ \pi \quad \text{for} \quad B > 1/(1-A'). \end{array} \right\} \quad (36)$$

When no such angles do exist the proper angles to be inserted in the following integrals are given. This occurs in the two simple cases of regions I and II in the A—B plane.

The expressions for the sums of areas in Fig. 2 then lead to

$$\left. \begin{aligned} g(A, B) &= \int_0^{\pi/2} \frac{1}{2\pi} A_3 \sin\theta\, d\theta \\ &= \int_0^{\pi/2} \int_{\varphi'}^{\pi} (2-L) \frac{d\varphi}{2\pi} \sin\theta\, d\theta \\ &= \int_0^{\pi/2} \left\{ \frac{\pi - \varphi'}{\pi} - \frac{2B}{\pi} \left[E\left(k, \frac{\pi}{2}\right) - E\left(k, \frac{\varphi'}{2}\right) \right] (1+A') \right\} \sin\theta\, d\theta \end{aligned} \right\} \quad (37)$$

and

$$\left. \begin{aligned} h(A, B) &= \int_0^{\pi/2} (1/4\pi)\,(A_4 + A_5) \sin\theta\, d\theta \\ &= \int_0^{\pi/2} \left\{ \int_0^{\pi} W\, d\varphi/4\pi + \int_{\varphi''}^{\pi} (2-\omega) \frac{d\varphi}{4\pi} - \int_{\varphi'}^{\pi} (2-L)\, d\varphi/4\pi \right\} \sin\theta\, d\theta \\ &= (B/4\pi) \int_0^{\pi/2} \{ (1+A')\,[4E(k, \pi/2) - 4E(k, \varphi'/2) + 2E(k, \varphi''/2)] \\ &\quad - 2\pi + \varphi'' + (2/B)\,(\varphi' - \varphi'') + A' \sin\varphi' \} \sin\theta\, d\theta \end{aligned} \right\} \quad (38)$$

and

$$f(A, B) = 1 - g(A, B) - h(A, B), \quad (39)$$

where

$$E(k, \varphi) = \int_0^{\varphi} [1 - k^2 \sin^2 t]^{1/2}\, dt, \quad (40)$$

$$k^2 = 4A'/(1+A')^2. \quad (41)$$

When the particles have initially a distribution in velocity, the functions f, g, and h have to be integrated over this distribution. Such an integration is essentially an integration over A. When

there is a distribution in z_γ one has to sum over this distribution. Such a summation is a sum over different B values. Thus, the final expressions for the currents are given by

$$\left.\begin{matrix} i_- \\ i_+ \\ i_{\text{out}} \end{matrix}\right\} = \sum_{z_\gamma} n_{z_\gamma}\, z_\gamma \int P(u) \left\{\begin{matrix} f(A,\,B) \\ h(A,\,B) \\ g(A,\,B) \end{matrix}\right\} du \cdot Ne \qquad \left.\vphantom{\begin{matrix} a \\ b \\ c \end{matrix}}\right\} \quad (42)$$

which, under the proper conditions, leads to the approximations (50) and (51) of ref. 2 (cf. also eq. (44) of ref. 2 and the series expansion of the function $S(A)$ in Appendix A).

If experimentally one is mainly interested in the velocity spectrum, one obtains the best results by measuring along B = const. curves in the A—B plane. When the highest accuracy is desired in the charge distribution, it is convenient to measure along $\langle A\rangle$ = const. curves in the A—B plane. In the present experiments, we have confined ourselves to an approximation to the latter procedure by measuring along curves for constant V, i. e., along curves of the type

$$B = \text{const}/\langle A\rangle^2. \qquad (43)$$

Therefore most information is available about the charge distribution and only $\langle u\rangle$ is obtained. So far nothing is known about the u distribution, which in the present experiments was considered to be a sharp line (cf. section 3.1).

1.4 An Example in which $V < T_R$.

If no magnetic field is applied, the expression for i_+ as a function of V can be found from eqs. (1) and (3) of ref. 2. We find

$$i_+ = \sum_{z_\gamma} n_{z_\gamma} \cdot z_\gamma \left\{\begin{matrix} T_R/(6\, z_\gamma\, eV) & \text{for } eV \geqslant T_R/z_\gamma \\ \frac{1}{2}\left(1 - \frac{2}{3}\,[z_\gamma\, eV/T_R]^{1/2}\right) & \text{for } eV \leqslant T_R/z_\gamma. \end{matrix}\right\} \quad (44)$$

In Fig. 3, this expression is plotted as a function of T_R/eV for singly charged atoms (curve A).

If a small magnetic field is applied, we obtain in the region

$eV \geqslant T_R/z_\gamma$ the approximation (44) of ref. 2, corresponding to the series expansion of $S(A)$ given in Appendix A. Furthermore, we know the asymptotic behaviour of i_+ for $V \to 0$ which is given by the series expansion (17) of ref. 2. This expression we multiply by 1/2 in order to change to the variable H_1' which we use here.

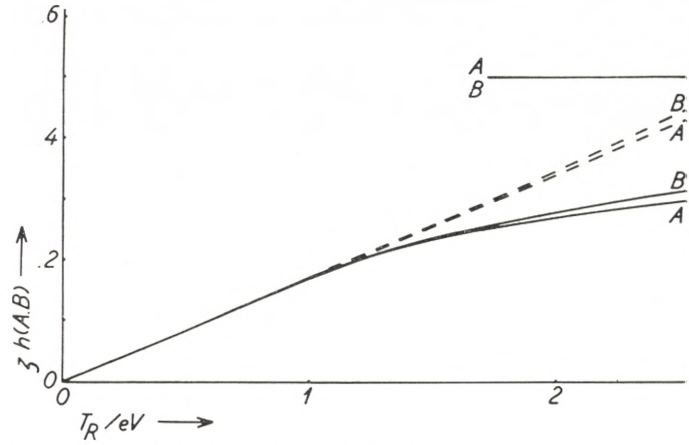

Fig. 3. Theoretical expectations for i_+ as a function of T_R/eV in a pure electric field (curve A). If a small magnetic field is applied, small changes in the curve appear. The general appearance is, however, the same. The curve B corresponding to 9.6 eV recoils with charge $z = 1$ and mass 37 amu. has been drawn by joining the known behaviour of the curve for $T_R/eV < 1$ to the known asymptotic behaviour for $V \to 0$. It should be noted that an upper limit to the deviation from curve A lies around (1/20) A^2 (cf. eq. (88) of Appendix A). Particles of the same energy and mass, but of higher charge, will follow the dotted curve.

We shall be interested in the behaviour of 9.6 eV singly charged particles of mass ~ 37 amu. moving in a magnetic field $2aH$ of 475 Gauss cm. In this case, the corrected curve for $eV > T_R$ is shown in Fig. 3 curve B, together with the asymptotic behaviour for $V \to 0$. Instead of carrying out long calculations inside the region IV of Fig. 27, Appendix A, we are content with the approximate curve B in Fig. 3, which is drawn loosely to fit the known behaviour in both ends. Such a procedure is of course rather uncertain. We are interested in the deviation from the dotted continuation of the straight line valid for $eV \geqslant T_R$ and we need this deviation only to an accuracy of ~ 10 pct. Thus, the present rough approximation is justified.

1.5. Motion of the Electrons.

The motion of the electrons is described in ref. 2. We are especially interested in the approximative expression (49) of ref. 2. In our case, we are dealing with $N\langle z_\gamma\rangle$ electrons. Thus, we get

$$i_{\pm e} = -Ne\langle z_\gamma\rangle\,[\pi\langle p_e c\rangle/(8aHe) \pm F\langle W_e\rangle/(2aH^2e) + \cdots]. \quad (45)^1$$

For the current i_{out} we get, to the same approximation, i. e., to second order terms in F/H,

$$i_{\text{out}\,e} = -Ne\langle z_\gamma\rangle\,[1 - \pi\langle p_e c\rangle/(4aHe) - \cdots]. \quad (46)$$

The expressions (45) and (46) are valid only when $eHa > cp_e^{\max}$.

Let us consider n electrons of definite momentum p and, as usually, created uniformly throughout our space between the infinitely extended condenser plates. In a pure magnetic field, we get the total expression covering all H values by combining (13) and (16) of ref. 2 or using (50) of the present paper

$$i_e = \begin{cases} en\pi\langle cp\rangle/(8aHe) & \text{for } Hea \geqslant cp \\ (ne/4)\{[1-(Hea/cp)^2]^{1/2} & \\ \quad + (cp/Hea)\,\text{Arcsin}\,(Hea/cp)\} & \text{for } Hea \leqslant cp. \end{cases} \quad (47)$$

This expression is illustrated as a function of pc/Hea in Fig. 4, curve A.

In the following, we are dealing with electrons of kinetic energy $T_e = 2300\ eV$ moving in an electric potential $V = 30\ eV$. In order to calculate the exact curve in this case, we would have to apply formulae like those given in (37)—(39) with very high A values and even calculated in the region V of the A—B plane. For $Hae > pc$, we can apply (45) and, for $H \to 0$, we know the asymptotic behaviour from the expression (3) of ref. 2 or (44) of this paper. Curve B in Fig. 4 is drawn in this way by fitting to the known behaviour in both ends. This procedure is of course uncertain. If a larger number of electrons with smaller energy contributed to i_e, the curve would continue along the dotted

[1] In equation (49) of ref. 2, a factor $^1/_2$ is missing in the first term. Also the five last lines, including eq. (20) on page 13 of ref. 2, are wrong and should be omitted.

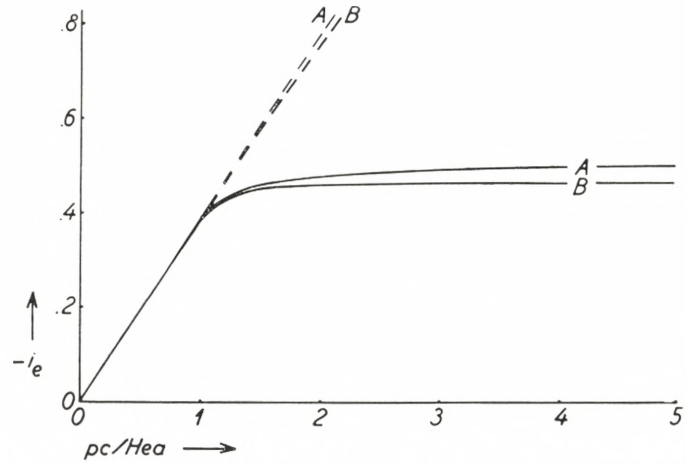

Fig. 4. i_e as a function of pc/Hea for electrons moving in a pure magnetic field (curve A). If a small electric field is applied, changes like those leading to curve B are assumed to appear.

line B which is obtained from (45). The actual curve deviates from this line; we shall use this deviation to an accuracy of 8 pct. only. Therefore it is felt to be safe to apply curve B without carrying through long and laborious calculations.

1.6. Pressure Effects.

When the positive particles collide with residual gas molecules, their charge and momentum are changed, and the current measurements are thereby distorted. We shall not attempt to give a detailed calculation of the complex phenomena occurring in such cases. We only note that pressure effects must be eliminated by carrying out measurements at various pressures and extrapolating to zero pressure.

Order of magnitude estimates of pressure effects are to be found in ref. 2, p. 18 ff. The considerations given there apply to singly charged particles. In the present investigation we are concerned with one more effect connected with pressures, which we will consider now. This effect occurs when a highly charged particle captures an electron, afterwards the fields act on it with reduced strength. A particle which otherwise would

have moved out towards infinity may thereby hit the collector plate. This effect is even increased by the possibility that the particle undergoes several such capture processes.

The pressure is expected to have influence when many particles spiral out. When H and V have such values that no particles can spiral out, the path of the recoils is very short and the pressure effect is a minimum. When particles spiral out, longer orbits occur and particles from the guard ring regions may have to pass the collecter region, thereby creating additional possibilities for such effects. This means that the guard ring regions should not be made too large. On the other hand, application of crossed electric and magnetic fields means that all particles obtain an average velocity in the y-direction given by

$$\langle v_y \rangle = Fc/H. \tag{48}$$

This velocity is larger than the recoil velocity by a factor $1/A$. Therefore the particles are very swiftly removed towards the walls of the chamber, and pressure effects are suppressed.

The worst case obviously occurs when $F = 0$. Then even standing orbits appear. Such particles are of course bound to collide. A good idea of the difficulties arising in this case may be provided by the following naive picture. Suppose that the main effect is charge changes and that the averaging mechanism of the instrument completely averages out the momentum changes. Suppose that this includes the gas molecules delivering the charge in question in such a way that the mathematics is defined as follows. Particles hitting a plate before a complete revolution in the motion in the $x - y$-plane are not affected by pressure. Particles which spiral up or down between the plates may capture an electron, but continue with the same momentum. The particle from which the electron is captured receives so little velocity from the capture process that it is sent out towards infinity with no possibility of hitting the collector.

Furthermore, we assume that the condenser is 2×1 cm long and that we are collecting in an infinitesimally thin region of the condenser only. Finally we also assume that the charge changes by one unit at a time. Then we get the following contributions to the currents to the plates:

$$i_1 = \sum_{z_\gamma = 1} n_{z_\gamma} z_\gamma j\,(pc/Heaz_\gamma), \tag{49}$$

where $j(pc/Heaz_\gamma)$ is given by

$$j_{z_\gamma}\,(pc/Heaz_\gamma) = 1/2 - \int_0^{\theta'_{z_\gamma}} [(a - \varrho_{z_\gamma})/2\,a] \sin\theta\, d\theta, \tag{50}$$

where

$$\varrho_{z_\gamma} = pc \sin\theta/(Hez_\gamma) \tag{51}$$

$$\theta'_{z_\gamma} = \left\{ \begin{array}{ll} \text{Arcsin}\,[Hez_\gamma/pc] & \text{for } Heaz_\gamma \leqslant cp \\ \pi/2 & \text{for } Heaz_\gamma \geqslant cp \end{array} \right\} \tag{52}$$

(cf. eqs. (13) and (16) of ref. 2). Eq. (49) gives the contribution from those particles which hit the collector before fulfilling one complete revolution. When the integrations in (50) are carried out we obtain (47) of the preceding section.

The contribution to the current from the particles changing charge from z_γ to $z_\gamma - 1$ is then given by

$$i_z = \sum_{z_\gamma = 2} (z_\gamma - 1)\, n_{z_\gamma}\, k\left(\frac{pc}{Heaz_\gamma},\ \alpha_{z_\gamma}\right), \tag{53}$$

where

$$\left. \begin{array}{l} k\left(\dfrac{pc}{Heaz_\gamma},\ \alpha_{z_\gamma}\right) = \displaystyle\int_0^{\theta'_{z_\gamma}} \frac{a - \varrho_{z_\gamma}}{2\,a} \left(1 - e^{-\alpha_{z_\gamma}/\cos\theta}\right) \sin\theta\, d\theta \\ \qquad - \displaystyle\int_0^{\theta'_{z\gamma-1}} \frac{a - \varrho_{(\gamma-1)}}{2\,a} \left(1 - e^{-\alpha_{z_\gamma}/\cos\theta}\right) \sin\theta\, d\theta \end{array} \right\} \tag{54}$$

and $\alpha_{z_\gamma} = 1/\lambda_{z_\gamma}$, where λ_{z_γ} is the mean free path for a z_γ fold charged ion.

Further contributions from additional charge changes are determined by calculations similar to those involved in the description of a successive radioactive decay. All integrals involved will contain expressions of the following kind only:

$$\int_0^{\theta_{z_\gamma}} \sin^2\theta \left(1 - e^{-\alpha/\cos\theta}\right) d\theta, \tag{55}$$

$$\int_0^{\theta_{z_\gamma}} \sin\theta \left(1 - e^{-\alpha/\cos\theta}\right) d\theta. \tag{56}$$

The integral (56) can be expressed in terms of known functions (exponential integrals). The functions have been tabulated as functions of θ_{z_γ} and α[1], however, in the present rough treatment the deviations from (50) can be neglected. Thus, the resultant current is still of the form (49), but more complicated expressions are entering (instead of the factors n_{z_γ}).

It is therefore to be expected, at least at not too high pressures, that the main characteristics of (49) appear, although the interpretation of the magnitude of the different charge components is more doubtful. Then only the possibility of determining the momentum of the recoils from the shape of (49) remains. (Cf. Fig. 7 of ref. 2).

One of the above conditions seems not to be fulfilled experimentally, namely, the condition that the molecules from which the charges are taken spiral out; however, it is likely that a diffusion of these ions occurs, giving rise to a constant positive current. This current is not affected by the magnetic field when $Hea > pc$.

The only safe procedure is certainly to carry out experiments at various pressures and to extrapolate to zero pressure.

Chapter 2. Construction of the Instrument.

2.1. The Magnet.

The instrument is shown in Fig. 5. Its main parts are: the magnet with its stabilized generator (A, N). The main vacuum chamber containing the collector system (not visible in Fig. 5), the electrical equipment for measuring small currents and for generating the potential V (B, C, F, J, R), the vacuum system

[1] The authors are indebted to civ.ing. K. O. Nielsen and fil. lic. G. Ehrling for tabulating the functions (55) and (56) on the electronic computor Besk in Stockholm, Sweden.

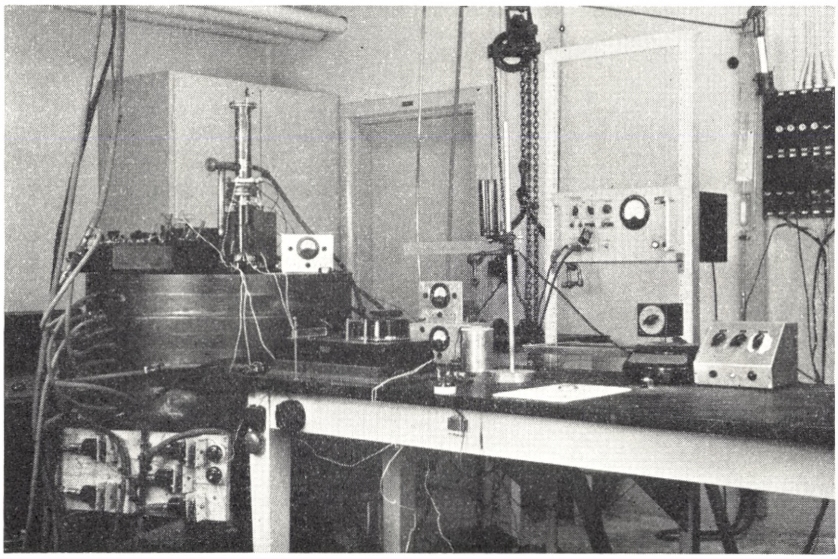

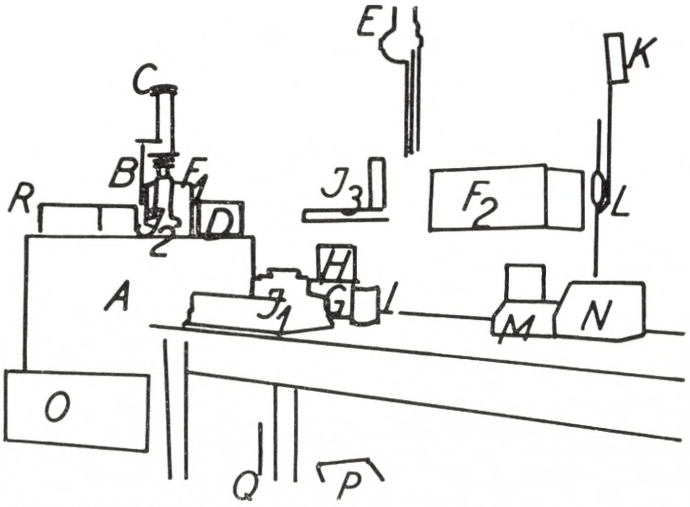

Fig. 5. General view of the instrument. *A*. Magnet. *B*. Vacuum tube with wire connection from the central part of the collector plate to the condenser *C*2 and to the vibrating reed electrometer. *C*. Vacuum container for the condenser *C*2. *D*. Pirani gauge for *Ca* furnace 2. *E*. Crane. F_1. Vibrating reed electrometer with preamplifier. F_2. Main amplifier and power supply for vibrating reed electrometer. *G*. Penning gauge. *H*. Forevacuum Pirani. *I*. Ice container for thermoelement. J_1. Compensation instrument *P*2. J_2. Galvanometer belonging to J_1. J_3. Galvanometer scale and lamp belonging to J_1. *K*. Liquid air trap. *L*. McLeod gauge. *M*. Galvanometer for thermoelement reading. *N*. Current adjuster for magnetic field. *O*. Water relais with alarm bell. *P*. Diffusion pump. *Q*. Mechanical pump. *R*. Resistances and voltmeter giving *P*2 and *P*4.

and devices for keeping the pressure down without actual pumping (not visible in Fig. 5).

The magnet was constructed by T. B. Thriges factories, Odense, Denmark. The other parts of the equipment were built at this institute.

The magnet is shown in Fig. 6. The iron surrounds a cylindrical gap, which contains the coils with their water cooling and

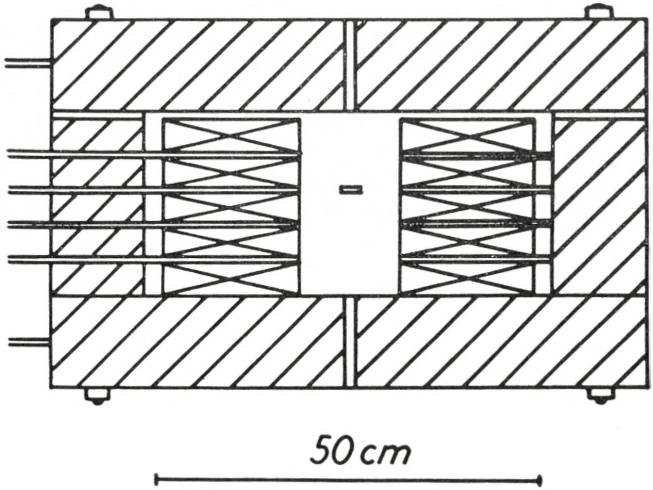

Fig. 6. General diagram of the magnet with coils, water cooling etc.

insulation system. A small cylindrical air gap, 13 cm in diameter and 24 cm long, is left. This air gap constitutes the essential space into which the main vacuum system is introduced. The coils are made of 20 times 1 mm^2 flat copper wires insulated with plastic materials. 10 such flat coils are placed above each other, and between every second coil a water cooled plate is introduced. The magnet is very compact, which involves some difficulties when the main instrument is to be inserted. The main advantage of this construction is the relative cheapness of the magnet. Vacuum and electric and mechanical connections are made through narrow channels in the lid and bottom of the magnet and in one of the cooling plates.

The magnet is fed from a *DC* generator, which is stabilized in the standard manner applied in this institute[3]. The homogeneity of the field is measured by moving small test coils up

and down and in the radial direction inside the air gap. The largest inhomogeneities appear around the narrow channels leading into the air gap through the bottom and lid of the magnet. These inhomogeneities do not extend far enough to be of any significance for the main instrument, which, due to the thickness of the vacuum chamber, first begins at about 2 cm from these channels. Apart from these inhomogeneities, slight inhomogeneities of up to 1 pct. appear, making the field slightly weaker in the central plane of the equipment. This is not very satisfactory and it will be seen later that these field inhomogeneities in fact are responsible for the most important source of systematic errors in the measurements.

The linearity of the magnetic field with the input current was investigated by means of a magnetic weight introduced in the air gap and with the possibility of balancing through the air gap between the uppermost coil and the iron lid. The investigation has shown that the field varies linearly with the current to within .1 pct. throughout the whole region applied here (up to 13000 Gauss). The remnant was found to be negligible.

The absolute calibration of the field was taken from a calculation on the magnetic and electric circuits. In fact, this calibration is not necessary, since it can be provided by means of the results (61 a) and (77). An error in the calibration would affect these two results in opposite directions.

In the following, the magnetic field was always taken from the measurements of the current in the magnet and calibrated in the above mentioned manner.

The water cooling of the magnet was not adequate for keeping the temperature constant in the air gap. This is another important source of possible systematic errors in the measurements, although it has been largely reduced by inserting an additional water cooled shield between the coils and the vacuum chamber.

2.2. The Collector System.

The collector system is shown in Fig. 7. The whole system is placed in the magnetic field generated in the magnet Fig. 6. A water cooled brass shield *C* is introduced between the coils

and the main instrument. This meant an essential improvement of the instrument. However, even with this extra cooling, the temperature varies when the field operates for a long time. If, say, 70 amps are sent through the coils, the temperature increases by about 35° C during 30 minutes when no water is sent through the channels of the shield, and by about 3° C when the

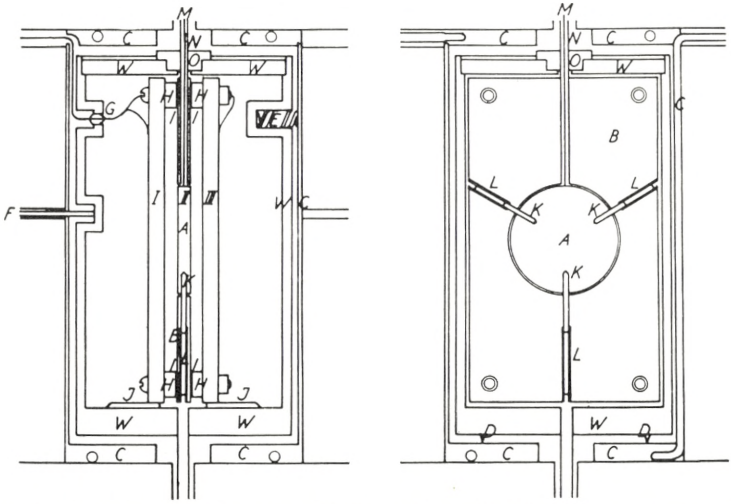

Fig. 7. The vacuum chamber and collector system. I and III. The outer electrodes. II. The inner electrode. *A*. The collector. *B*. The guard ring. *C*. Water cooled shield. *V*. Vacuum chamber. *D*. Pivots. *E*. Phosphor bronze spring. *F*. Micrometer screw. *G*. Glass insulator. *H*. Brass stopper. *I*. Polystyrene foil. *J*. Perspex insulator. *K*. Textolite insulators. *L*. Brass screws. *M*. Connection to vibrating reed. *N*. Guard ring tube. *O*. Perspex insulator.

shield is cooled. The temperature is measured in the space between the shield and the vacuum chamber *W*.

The collector system is contained in the vacuum chamber *W*. *W* rests on the two pivots *D* and is kept in position by the phosphor bronze spring *E* and the micrometer screw *F*. When the system is put together, vacuum established and A^{37} introduced, the entire system can be tilted so that the collector plates can be adjusted parallel to the lines of force of the magnetic field (cf. section 2.6).

The collector system consists of a double condenser. Duplicity is only introduced for convenience. The two outer condenser plates I and II are short circuited, and the central condenser plate II is supported by .700 cm brass stoppers *H* and .004 cm

polystyrene foils I, which provide the insulation between I and III and the guard ring part *B* of II. The plates I and III rest on perspex insulators *J*. The whole system is screwed together so that no displacement occurs when the instrument is tilted.

The central part *A* of plate II is the essential collector. It is carefully insulated from *B*. Insulation is provided by the three textolite insulators *K*, which are pressed into position so that *A* and *B* are perfectly plane. The insulators are pressed in position by the brass screws *L*. *A* is connected to the vibrating reed electrometer by means of the thin wire *M*, which is brought out through a thin hole drilled in *B* and completely filled with insulating material, so that A^{37} cannot penetrate into this space and cause false currents. Finally, the insulator is vacuum sealed to the wire and to the thin brass tube *N*, which provides the electric guard ring for the collector connection. *N* is silver soldered to *B* and brought out through the insulator *O*, thus giving the possibility for electric contact to *B*. All electric connections inside the evacuated parts are soldered. This is a very important precaution in order to avoid false potentials due to accidental disconnections when vacuum is established. The inside of the vacuum chamber and of I, II and III is covered with a thin layer of gold in order to minimize effects from surface potentials. Care was taken to make the insulators (as seen from the inside of the system) as small as possible. Such insulators may be charged by the currents and thereby distort the electric field. The dimensions of the instrument are chosen so as to fulfill the conditions (21), (22), and (23) of ref. 2 in order that the central part *A* of the collector represents part of an infinitely extended condenser in all experiments discussed here. At the same time, sufficient homogeneity of the electric field is obtained.

The outer part *B* of the central plate acts as a guard ring and is kept at the same potential as the collector *A*. Nevertheless, contact potentials may cause small currents over the many insulators between *A* and *B*. A special investigation was carried out with the aim of finding insulators which are both rigid enough mechanically and sufficiently well insulated even when they are strongly irradiated with *X*-rays. This investigation is described in Appendix C. Textolite was found to fulfill these conditions.

2.3. The Electrical System.

The wire M of Fig. 7 is connected to a vibrating reed electrometer in the manner shown in Fig. 8. The connection is carried out in a metal vacuum container. Metal was chosen

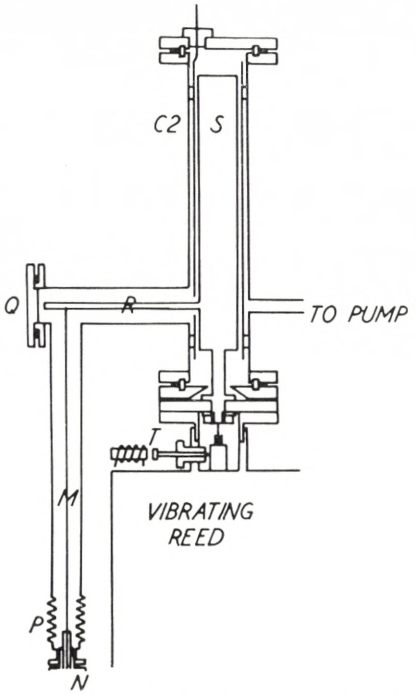

Fig. 8. Connection to vibrating reed, condenser $C2$ and magnetic switch. M. Wire from the collector A of Fig. 7. P. Metal bellows. Q. Flange. R. Rod fixed to the central plate of $C2$. S. Central electrode of $C2$. T. Magnetic switch.

because the collector system has to be shielded from disturbing electric potentials. The vacuum is necessary in order to ensure that this system should not act as an ionization chamber for cosmic rays or radioactive impurities. The vibrating reed is used as a zero indicator only, and the charge arriving at M from the collector is neutralized by charging the additional condenser $C2$ from a compensation instrument.

Again all electric contacts inside vacuum are soldered, and current is drawn through all connections in order to ensure contact. The membrane P provides the flexibility needed in order

that the main vacuum chamber can be tilted without disturbing the secondary vacuum in the system shown in Fig. 8. The flange Q is only introduced in order to enable us to put the instrument together and to solder M to the fixed rod R which leads to the inner electrode 5 of $C2$. The additional condenser $C2$ rests with its inner electrode in the socket of the vibrating reed electrometer. The magnetically operated switch T makes it possible to set the system free and ready for measurement.

Fig. 9 shows the circuit diagram with the same notation as

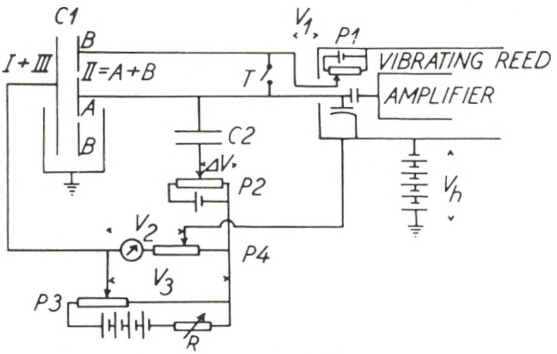

Fig. 9. The circuit diagram.

used previously. The outer condenser plates are connected to a battery of dry cells. The potentiometer $P1$ generates the potential V_1 on A and B.

V_1 is chosen such that it equals the contact potential between the reed and anvil in the vibrating reed electrometer. Thereby the reed indicates zero potential. When the short circuit T is removed the inner system is free and completely insulated from all other conductors in the instrument. $P2$ gives the compensation potential 0—1 volt on $C2$ which is used to keep the reed showing zero when ions are collected on the collector. The time t it takes to charge $C2$ to, say, 1 volt is a measure of the currents i_+ or i_- given in Chapter 1. $P3$ gives the possibility of generating a variable potential V_3 between certain parts of the instrument. V_3 can be adjusted for long time drift by means of the variable resistance R. $P4$ divides V_3 so that a certain portion of V_3 is connected to $C2$ and the remainder, V_2, is the essential part of the potential V between the outer and inner plates of the collector system. $P4$

is adjusted so that a variation of V_3 causes no indication on the reed. The principle of this procedure is illustrated in Fig. 10. When V' is changed, say, from 0 to W volts, a voltage change in the vibrating reed is measured. This voltage change ΔV is given by

$$\Delta V \cong - W \frac{\Delta}{R_1 + R_2} \frac{C_2}{\Sigma C_i}. \tag{57}$$

ΣC_i is the sum of various capacitances between the insulated system and all other parts of the instrument.

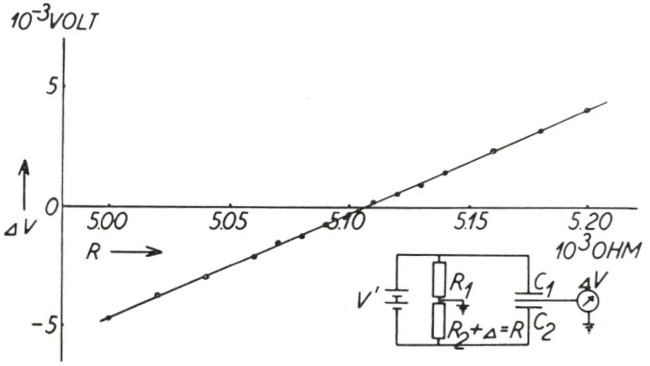

Fig. 10. Indication on vibrating reed for a 3 volt variation of V_3 as a function of the resistance R. Basic circuit diagram is shown.

In Fig. 10 are also given the measured results for ΔV as a function of $R = R_1 + \Delta$ when V' is varied from 0 to 3 volts, which is far more than any drift during a single experiment. It is seen how complete compensation can be obtained by putting $R = 5107$ ohms. Now measurements can be carried out at a potential $V = V_1 - V_2$ across $C1$.

The condenser $C2$ is about 60 cm. Therefore, a current of 10^{-14} amp will cause a charging to 0.1 volt in approximately 300 sec. Such an interval of time can be measured by means of a stopwatch with an accuracy of 0.2 sec. Thus it is possible to measure currents of this order with an accuracy of 0.1 %. The zero current of the entire instrument, when radioactive Ca is placed in the Ca furnace 2 described in 2.5, is $< 5 \cdot 10^{-18}$ amp and the instrument noise is $< 10^{-4}$ volts which, together with the uncertainty in the time measurement, still permits a 0.1 accuracy.

2.4. The Potential V_h.

When electrons move in our crossed electric and magnetic fields we can, as mentioned in 1.5, practically neglect the influence of the electric field. An electron will thus essentially move in helical orbits. If the electron is created at a point with positive potential, it will not be able to spiral out towards the

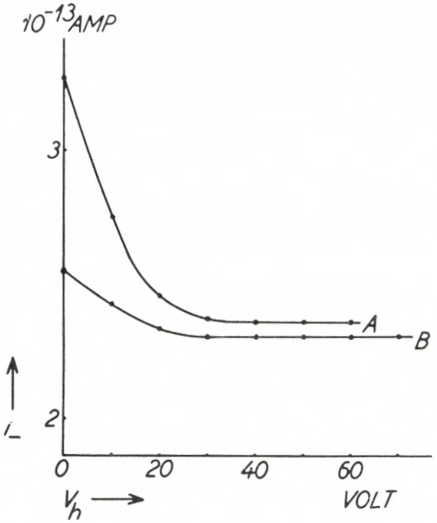

Fig. 11. The figure shows $i_{\_}$ as a function of V_h for $V = 34$ volts and $H = 1450$ Gauss. Curve A corresponds to a pressure of $2 \cdot 10^{-4}$ mm Hg, curve B corresponds to $3.6 \cdot 10^{-5}$ mm Hg.

lid and bottom of the chamber, unless the lid and bottom are placed at a positive potential of approximately the same value as, or a higher value than, that at the point where the electron is created. The effect is similar to that which is utilized in the Penning manometer.

This situation occurs especially when the collector is at zero potential and the plates I and III are at positive potentials. In this case, the electrons will travel up and down in the instrument until they change momentum by collisions with molecules of the residual gas. Thereby the electrons may ionize the molecules giving a new charge which is collected and which falsifies the current measurement.

The effect can easily be removed by applying the potential V_h as shown in Fig. 9. In Fig. 11 the effect of V_h is illustrated. A^{37} has been enclosed in the vacuum system in the manner described in the following, a magnetic field and an electric field of $V = 34$ volts are applied. The current observed is then described as a function of V_h. It is seen that too high positive currents are obtained until $V_h > 34$ volts, i. e., until no electrons are created at higher potential than the potential at the bottom and lid of the vacuum chamber. The curves in Fig. 11 refer to two different values of the pressure, and it is seen that the effect is more pronounced for higher pressures. This is of course a support for the whole picture of the effect.

As a consequence of the present results, V_h was always kept slightly above V in the following experiments. The procedure is not quite satisfactory and, in future instruments of this type, it will be necessary to deal with the fields at the limits of the collector system in a more satisfactory way. Either one field should be applied so as to remove the heavy particles and, as here, the lid and bottom of the instrument kept at a potential V_h, or else a more continuous termination of the electric field should be provided.

2.5. The Vacuum System.

The auxiliary vacuum system is illustrated in Fig. 12. The tube leading from the bottom of the main chamber in Fig. 7 is through a joint U connected to the quartz tube Y containing commercial Ca. The Ca is heated continuously by a stove which is not shown in the figure. In this way, Ca acts as a getter, and the pressure can be kept down in the main instrument for rather long periods of time. A stopcock V leads to a closed system consisting of a stainless steel tube X, which contains 5 g of Ca irradiated for four weeks in the Harwell pile. This Ca contains some millicuries of A^{37}. The closed system also contains a Pirani gauge W. Another stopcock Æ leads to the Penning gauge. Ø leads to the vacuum pumps, consisting of two oil diffusion pumps and a mechanical pump. Å leads directly to a liquid air trap and further to a McLeod manometer. The liquid air trap prevents Hg vapour from spreading out in the instrument.

When X is heated, A^{37} is liberated and, thus, A^{37} can be introduced into the system. During heating, the pressure rises to very high values inside the closed system defined by V. However, as heating goes on, the pressure again is reduced and, when heating is interrupted, the pressure is further diminished.

When the main system has been pumped down for some time, and the Ca furnace Y has been heated continuously, it is

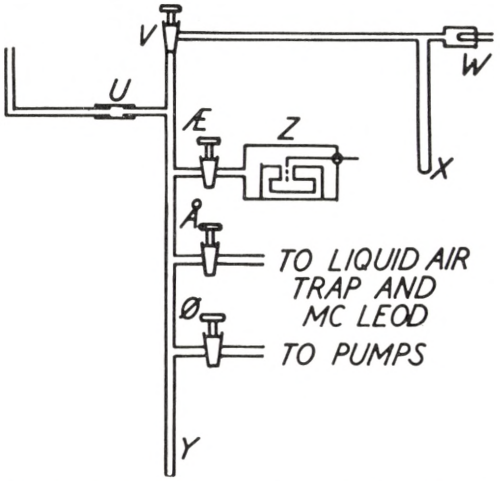

Fig. 12. The auxiliary vacuum chamber. *U*. Joint. *V*. Stopcock. *W*. Pirani gauge belonging to calcium furnace 2. *X*. Calcium furnace 2. *Y*. Calcium furnace 1. *Z*. Penning manometer. *Æ*. Stopcock. *Ø*. Stopcock. *Å*. Stopcock.

possible to keep the pressure down at 10^{-6} mm Hg, as read on the Penning gauge, for many days with the stopcock $Ø$ to the pump closed. Part of this is due, however, to the fact that the Penning acts as a pump. Gas molecules are ionized and bombarded into the pole pieces of the Penning magnet. This pumping action also diminishes the pressure of Argon, which is not taken by the Ca furnace. This is rather unfortunate since it means that also A^{37} is eaten by the Penning. Such an effect is clearly prohibitive for the entire experiment. That this is so was verified by a direct test using A^{37} as a tracer for A. The current i_- in the instrument was again measured for given values of V and H and followed through half an hour. The current was constant to within the above mentioned uncertainty. Then, as illustrated in Fig. 13, at the time $t = 0$, the stopcock $Æ$ was opened and the

Penning was permitted to operate. It is seen that the current i_- decreases within an hour to a fraction of the value it had before the Penning was allowed to eat A. The accuracy in the points after $t = 0$ is not too high because shorter time intervals than 300 sec were used for the measurements. Also, the operation conditions are more unstable in this case. The first very sharp

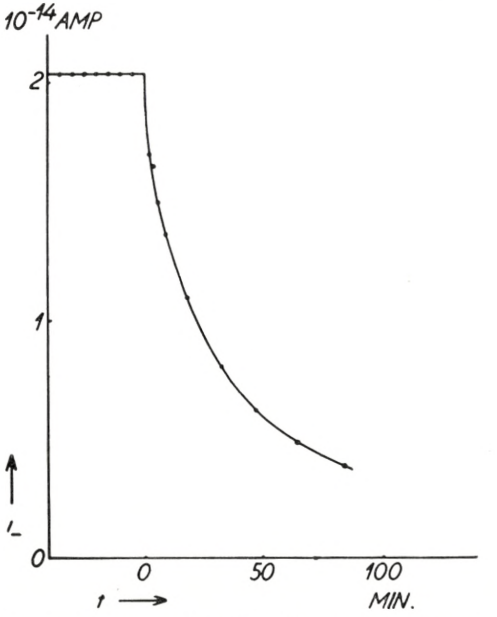

Fig. 13. The Penning manometer eats A. The figure shows the current i_- as a function of time t. At $t = 0$ the Penning is permitted to eat A.

drop is due to the fact that the Penning volume did not contain A^{37} before $t = 0$. It is of course impossible in this way to explain the continued decrease.

It was therefore necessary to use the McLeod only for the measurements of the pressure during the investigations. We could not obtain the very low pressures indicated above, but we had to work with the pressures which the *Ca* furnace alone could keep. It turned out that, with the present vacuum system, we had a practically constant increase of roughly 3—4 10^{-5} mm *Hg* per day when the Penning was not operating. This is presumably due to A leaking into the instrument. The pressure curve as a function of time is shown in Fig. 14. At $t = 0$, a portion of A^{37}

was introduced, and the pressure was rather high for the first few minutes. This is due to gas given off by the irradiated *Ca* when the furnace *X* is heated as mentioned above. After heating, the pressure in the closed system *X* did not go entirely down to zero. Part of this gas was, however, neutralized by the *Ca* furnace *Y*, and within half an hour the pressure decreased to

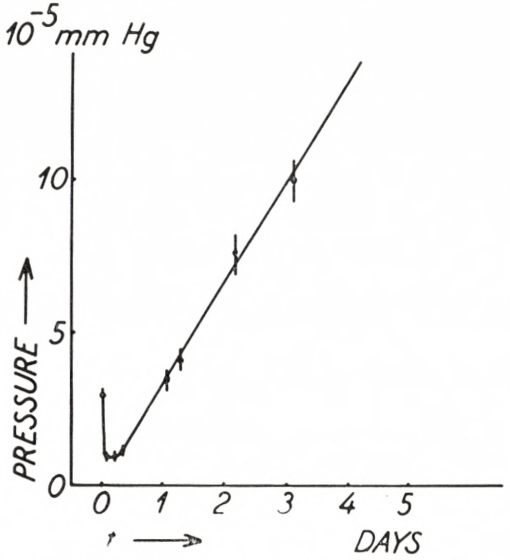

Fig. 14. Pressure in the instrument as a function of time after a portion of radioactive Argon has been introduced at $t = 0$.

a value slightly below 10^{-5} mm *Hg*, where it stayed for some hours. Thereafter, the pressure increased in the manner described above.

Two millicuries of A^{37} lead to a pressure of about 10^{-6} mm *Hg* in our approximately 2 liter vacuum system.

2.6. Tilting of the Instrument.

When the plane of the condenser is not parallel to the magnetic field, secondary electrons from the lid and bottom of the instrument spiral up and hit the collector. Thereby the currents to the collector are reduced. One can therefore directly use the current i_- as a function of the micrometer reading (Fig. 15) in order to get the best possible alignment of the instrument. In

the case illustrated in Fig. 15, the instrument has been inserted in the magnet in such a way that the tilting could not be carried further to the right because no more space was available in the two narrow channels of the pole pieces. In other investigations, the curve has been followed further to the right. The curve is thereby shown to be symmetric. If the field were homogeneous and the plates exactly plane, an effect proportional to the numer-

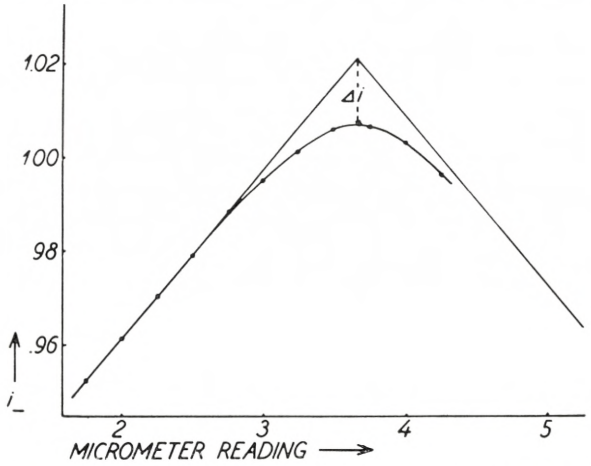

Fig. 15. Tilting of the instrument. The figure shows $i_{\_}$ as a function of the micrometer reading for $V = 60$ volts. $V_h = 70$ volts, $H = 4280$ Gauss, and at a pressure of 10^{-5} mm *Hg*. The currents are measured in the units used in the following, where $i_{\_}$ for $V = 30$ volts, $H = 2500$ Gauss has been put $= 1$. The current Δi is the deviation from the asymptotic behaviour. 1 unit micrometer reading corresponds to $\alpha = 25'$.

ical value of the tilting angle α would be expected, i. e., the deviation from the asymptotic behaviour of the curve is a direct measure of the influence of the inhomogeneities in the field and of the lack of planeness of the plates.

In our case, the field inhomogeneities are, as mentioned, so that the field is slightly weaker in the center of the air gap than at the position where the bottom and the lid of the vacuum chamber are placed. The effect is equivalent to the plates being curved away at the ends from the actual space utilized in the instrument. Thus, no shadow effect will occur when the chamber is tilted, and a simple argument shows that the asymptotes in Fig. 15 will intersect in the true point representing α_0 and that

current which would have been obtained if no field inhomogeneities existed. The current Δi thus represents the correction which must be applied on i in order to get the true i value when i is measured in the most favourable position of the instrument. Curves like that given in Fig. 15 were obtained for various values of H and V, but no variation could be found with certainty in Δi; hence, we have chosen to correct all our later measurements with the mean value observed, $\Delta i = .015$ in the standard units mentioned in the text to Fig. 15. This value is of course somewhat uncertain and must be taken with all due reservation. However, due to its apparent constancy, we need not be much worried when discussing small variations in H and V; furthermore, we have obtained an independent check on Δi in the arguments given in section 3.4.

2.7. Temperature Constancy.

Obviously, it is important to keep the temperature constant during the investigations, simply because the concentration of A^{37} is strongly affected if different parts of the equipment have differently varying temperatures.

This effect is illustrated in Fig. 16. The instrument was left for some days without cooling water so that room temperature was reached. When measurements were started (in the following referred to as the time $t = 0$), $V = 30$ volts and $H = 2500$ Gauss was applied and cooling water turned on; the curve shown in Fig. 16 was obtained, giving our standard reference current as a function of time measured in units 10^{-16} amp. The variation in temperature in the space between the water cooled shield and the vacuum chamber is also given in Fig. 16.

During the first few minutes after $t = 0$, the outer parts of the vacuum chamber are cooled down, whereas the collector system and the space between them stays at room temperature. Thereby the concentration of A^{37} between the plates is reduced, and the A^{37} concentrates in the outer parts of the vacuum chamber, where it is augmented until somewhat later, when the collector becomes cold and the relative concentration is restored. The final concentration is then slightly larger than the concentration at

$t = 0$ because the vacuum chamber now has a lower temperature relative to the *Ca* furnace, McLeod etc.

The uncertainties indicated in the current measurements in Fig. 16 are $2 \cdot 10^{-17}$ amp, representing 0.1 pct of i_-.

In the experiments described in the following chapter, the measurements have been performed by referring to the present

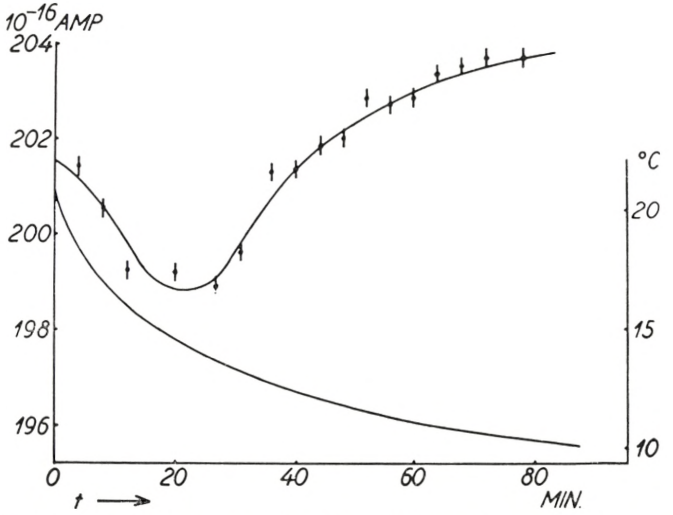

Fig. 16. The figure shows i_- as a function of time measured under our standard reference conditions $V = 30$ volts and $H = 2500$ Gauss. Also the temperature of the instrument is shown as measured in the space between the cooling shield *C* and the main chamber *W* (see Fig. 7).

values of V and H, putting the current obtained here $= 1$. The data have been taken by measuring the current for this value of V, H, for a new value of V, H, and then again for the present value of V, H and the result has been expressed as the ratio of the second measurement to the average of the first and last measurement. Occasionally, other reference values of V, H have been chosen, but then the new and the old reference points have been checked relative to each other before and after the set of measurements in question. Also each measurement has been repeated, and the results given later represent the average of the repeated measurements.

In this way, it is possible to eliminate the major effect of temperature changes and, simultaneously, the effects from the

decay of A^{37} leading to a decrease in concentration are eliminated.

It should be noted that the temperature changes observed in the present experiment are considerably larger than those encountered when the instrument is already cooled down. (Cf. section 2.2).

2.8. Statistics.

The currents observed vary from 0 to approximately $2 \cdot 10^{-13}$ amp. The latter current corresponds roughly to $1.2 \cdot 10^{6}$ electronic charges per sec., or to approximately $4 \cdot 10^{5}$ individual events per sec., if we put the average charge of the recoils to around 3 elementary charges (cf. section 3.4). In order to get a 0.1 pct accuracy in the current measurements, it is necessary to measure for about 200 sec. Thus, the total number of events amounts to about 10^{8}, giving statistical fluctuations of about 10^{4}. For the small currents, the absolute magnitude of the statistical fluctuations is of course smaller.

This is more than satisfactory for the present investigation but, on the other hand, it shows that an improvement of more than a factor 5 in the accuracy cannot be gained, unless much more time is devoted to each measurement, regardless of any other possible improvement in measuring technique.

2.9. Dielectric Polarization.

When the voltage is suddenly changed, the residual components of the dielectric polarization causes small errors in the currents. The effect can be measured when no radioactivity is present by following the charging up of the collector system due to binding of charges in the two condenser systems $C1$ and $C2$. The effect is similar to that illustrated in Appendix C, but much smaller. The effect takes place in what little can be seen of the insulators inside the entire system and probably also in oxide layers on the surfaces of the condensers.

The essential effect is found to last less than 10 minutes. Consequently, all measurements involving changes in V were carried out after waiting approximately 10 minutes before

starting. Fortunately, this effect does not coincide with the demand of varying the magnetic field and thereby changing the temperature of the instrument, because all curves for varying V are obtained at fixed values of H.

The existence of a heating effect accompanying H changes, and of a dielectric effect accompanying V changes, is the reason why the measurements were carried out at constant H or at constant V, as shown in the following, instead of measuring at constant B and at constant A, as mentioned in section 1.3.

In future constructions of instruments of the present type such effects should of course be avoided.

Chapter 3. Results with A^{37}.

3.1. The Decay of A^{37}.

A^{37} is reported to decay into Cl^{37} by 92 percent K-capture and 8 pct L-capture and with a half life of 34^{d} [4]. Primarily, electrically neutral recoil atoms are formed. However, successive Auger effects and the charge change of the nucleus from $Z = 18$ to $Z = 17$ cause a considerable ionization within a very short time ($\sim 10^{-10}$ sec) after the decay. The $Cl^{37}(p, n)A^{37}$ threshold gives that 817 ± 4 keV is available for the K-capture. Of this, approximately 3 keV is spent in excitation of the electronic core of Cl^{37}.

The recoil velocity distribution is primarily a sharp line originating from the practically monoenergetic neutrino emission, but is smeared out by ~ 6 per cent due to the recoil from the Auger effect and by a similar amount due to the Brownian motion at s. t. p.

This spread will only cause a ~ 2 keV difference between $c\langle p^2\rangle^{1/2}$ and $\langle pc\rangle$, the magnitudes with which we are mainly concerned here. We shall therefore neglect the spread in all our expressions and apply the sharp line formulas only. In these formulas we will insert $\langle u\rangle$ everywhere instead of u. Actually, as mentioned in 1.4, the velocity distribution could in principle be found by the present method, especially if measurements were made at suitable A and B values. Due to the effects

mentioned in the preceding sections, it is best, however, that we confine ourselves to the charge distribution and to a measurement of $\langle u \rangle$.

3.2. The Currents as Functions of Medium *H* Values.

When a potential $V > T_R$ is applied across the condenser, the contribution to i_- or i_+ from the recoils is a constant for

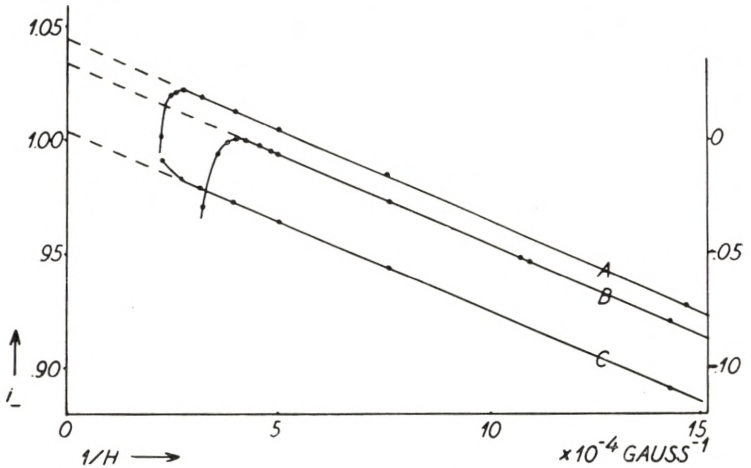

Fig. 17. Curve A: i_- as a function of $1/H$ for $V = 60$ volts, extrapolated to zero pressure, but without correction for Δi. Curve B: i_+ as a function of $1/H$ for $V = 30$ volts, extrapolated to zero pressure, but without correction for Δi. For curves A and B the ordinate is to the left. Curve C: i_- as a function of $1/H$ for $V = 60$ volts and at a pressure of 10^{-5} mm *Hg*, and without correction for Δi. For this curve the ordinate is to the right.

low H values (cf. eqs. (50) and (51) of ref. 2). The electrons, however, are collected according to (45) if H is not too small, i. e., to the first approximation we obtain for medium magnetic field currents of the form

$$i_\pm = A - B/H. \tag{58}$$

When i is plotted as a function of $1/H$ we should therefore observe a straight line. The results obtained are shown in Fig. 17 for $V = 60$, 30, and -60 volts. For the first two curves, a set of experiments has been performed at various pressures ranging

from $0.9 \cdot 10^{-5}$ mm *Hg* and upwards, and an extrapolation to zero pressure has been made. This extrapolation procedure is illustrated in Fig. 18. The magnitude of the correction which must be applied to measurements obtained at 10^{-4} mm *Hg* is shown in Fig. 19 for $V = 30$ volt and as a function of H. The correction varies linearly with the pressure for sufficiently low pressure values; it is seen that, for measurements performed at

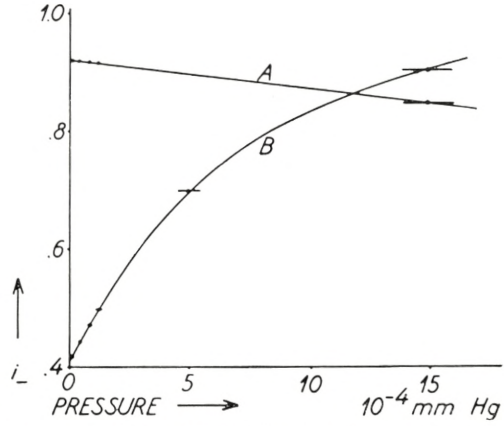

Fig. 18. Two pressure correction curves showing the maximum corrections needed in the present experiment. Both curves are obtained with $V = 30$ volts. Curve A corresponds to $H = 700$ Gauss. Curve B corresponds to $H = 6530$ Gauss. The points represent observed currents without corrections.

10^{-5} mm *Hg*, the corrections amount to 0.7 pct at most. Fig. 19 is an illustration of the effects discussed in 1.6. At $V = 2500$ Gauss, the positive particles begin to miss the negative plate and spiral out. Thereby the current is reduced and bends away from the straight line, as shown in Fig. 17. At the same time, a change in the behaviour of the pressure correction is observed, and this change clearly shows that pressure effects become more serious when the particles start spiralling.

Curve *C* in Fig. 17 is obtained at a pressure of 10^{-5} mm *Hg*. At this pressure, the pressure correction barely affects the straight line part of the curve. This curve bends upwards at approximately the same point where the curve *A* bends downwards, illustrating that particles missing the negative plate may sometimes hit the positive plate. The points where the deviation from

the straight line shape of the curves begins varies with V according to (42) of ref. 2.

$$\frac{2\,Mc^2V}{ez_\gamma(2\,aH)^2}\left(1-\frac{H}{F}\frac{u}{c}\right) = B_{z_\gamma}(1-A) = 1\,, \tag{59}$$

where we have to put $z_\gamma = 6$ in order to obtain agreement with the energy value for the neutrino energy, as mentioned in section 3.1. This will be further illustrated in the following.

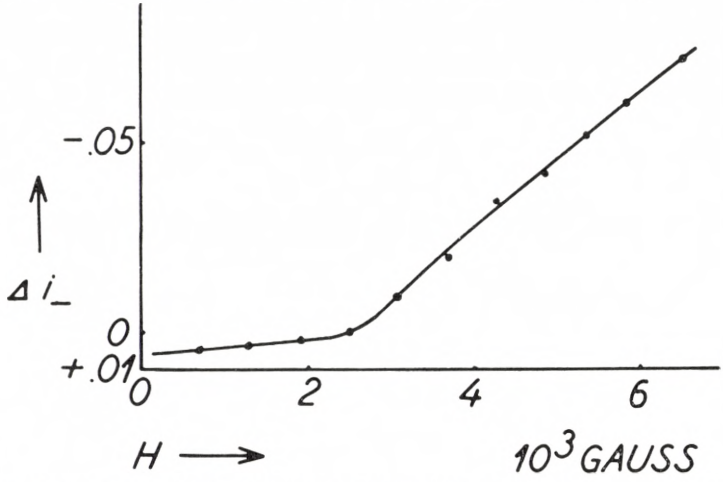

Fig. 19. The pressure correction to be applied to measurements carried out at $V = 30$ volts and a pressure of 10^{-4} mm *Hg*. The correction is given as a function of H.

From the curves in Fig. 17 it is apparent that the contribution from the electrons at higher values of H can be calculated as the difference between the end point value at $1/H = 0$ for the straight line extrapolated to this point and its value at the H considered.

Furthermore, the slope of the curve can be used to give the average momentum of all the electrons. The result is

$$Ne\langle z_\gamma\rangle\langle p_e\rangle \approx 1.071 \times (67 \pm 1)\ \text{Gauss cm}, \tag{60}$$

where we have written the result as a product of two numbers, thereby anticipating later results. Also, we have not used an equality sign in (60) because small corrections have to be taken into account (cf. section 3.5).

3.3. The Neutrino Momentum.

When H reaches a value corresponding to (59) for appropriate values of u and z_γ, some recoil particles contributing to i_- begin to miss the collector and either spiral out or add to the current i_+. As mentioned in the preceding section, this is the reason for the

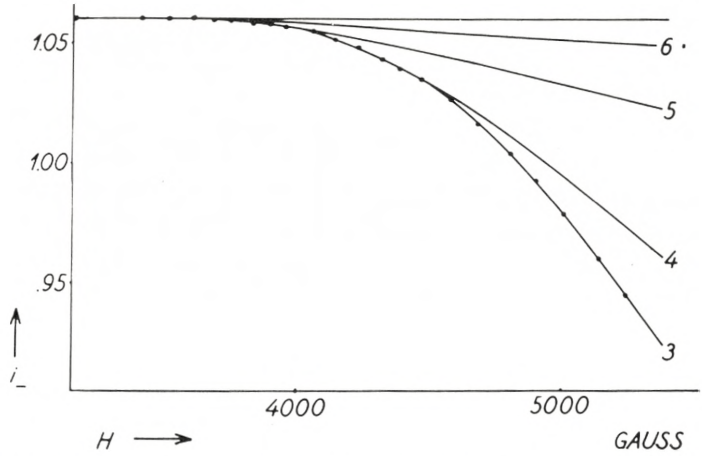

Fig. 20. Recoil contribution to i_- for $V = 60$ volts and as a function of H. The full drawn curves represent calculated contributions corresponding to the data in (61).

sharp drop in i_- and the slight increase in i_+ mentioned in connection with Fig. 17. In order further to investigate this effect we have measured i_- for $V = 60$ volts at higher values of H. The i_- values obtained have been corrected for the contribution from the electrons in the way mentioned in the preceding section. Also a contribution of .015 current units has been added in order to correct for the field inhomogeneity (cf. section 2.6). The results obtained in this way are illustrated in Fig. 20.

First, the data between $H = 3400$ Gauss and $H = 4500$ Gauss have been used to determine the momentum of the recoils. From our approximate knowledge of $Muc = 800$ keV from older recoil measurements[5] (cf. also section 3.6), or directly from the sequence of apparent humps in the curve in Fig. 20, it is possible to conclude that below $H = 4500$ Gauss only 4 or higher fold charged ions can miss the collector. Using the data in Appendix A,

we can thus calculate the contributions to the currents from 4, 5, 6, etc. charged ions with an assumed *Muc* value. Such calculations were carried out for a sequence of *Muc* values, and a least square fit was made of n_6, n_5, n_4 to each set of curves belonging to a definite *Muc* value. The sum of the squares of the deviations was calculated and the experimental data were found to agree with

$$\left.\begin{aligned} \langle Muc \rangle &= 812 \quad \pm 8 \quad \text{keV} \\ Nn_6 &= .004 \pm .004 \\ Nn_5 &= .015 \pm .005 \\ Nn_4 &= .075 \pm .008. \end{aligned}\right\} \tag{61a}$$

Proceeding with the set of curves for $Muc = 812$ keV, one finds from the data for $H > 4500$ Gauss

$$Nn_3 = .155 \pm .015 \tag{61b}$$

$$N(1.973\, n_2 + 0.973\, n_1) = .203 \pm .020. \tag{62}$$

The result for the *Muc* determination is rather insensitive to the pressure correction. This is quite natural because it merely depends on whether or not particles can spiral out. In other words, it depends on a comparison of H at the point where, say, 4 fold charged particles just begin to miss the collector with the value of H calculated from

$$\frac{Mc^2F}{4\,H^2a} = 1. \tag{63}$$

The deviation between these two H values is a direct measure of *Muc*.

Due to the large uncertainties in n_4 and n_5 it becomes very difficult to estimate n_2 by going to still larger values of H. We shall therefore proceed in a different manner in order to determine n_1 and n_2, namely, by finding N and $N\langle z_\gamma \rangle$.

3.4. The Average Charge.

When i_+ and i_- are measured as functions of V inside the interval where no recoils spiral out, results as those shown in Fig. 21 are obtained.

When $V > T_R/z_\gamma$, the curve should follow the expression (50)

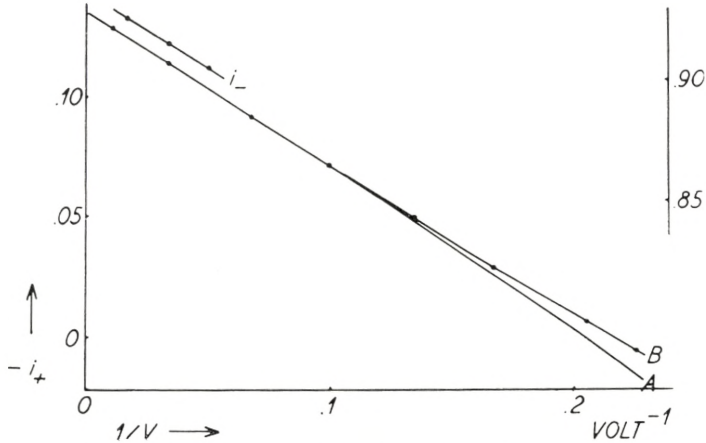

Fig. 21. i_- (scale to the right) and i_+ (scale to the left) as functions of $1/V$. The results represent directly measured currents at 10^{-5} mm Hg without correction for field inhomogeneities. Curve A is the expected curve if no singly charged resoils existed. $H = 675$ Gauss.

of ref. 2 (cf. also eqs. (85) and (88) of Appendix A). To the first approximation, we should thus expect

$$i_+ = -C + D/V. \tag{64}$$

Plotted as a function of $1/V$, a straight line results, as observed in Fig. 21. According to our considerations, $-C$ equals the contribution from the electrons at the magnetic field considered, i. e., at 675 Gauss. This contribution of course includes the current Δi due to field inhomogeneities. From Fig. 21 we obtain

$$-C = .136 \pm .001. \tag{65}$$

From Fig. 17 one obtains, by adding $i = -.014$,

$$-C = .135 \pm .001, \tag{66}$$

which shows that all currents present have been accounted for. This supports the interpretation of the tilting curve given in section 2.6.

The slope of the curve gives $Ne\langle T_R\rangle$. Since *Muc* is known, N can therefore be found. The result is

$$Ne = .405 \pm .008, \tag{67}$$

where the main uncertainty comes from the uncertainty in *Muc*. The data given in Fig. 21 and Fig. 17 also give $Ne\langle z\rangle$ which is found to be

$$Ne\langle z_\gamma\rangle = 1.071 \pm .001, \tag{68}$$

i. e., we obtain

$$\langle z_\gamma\rangle = 2.64 \pm .05. \tag{69}$$

We have now all the data required in order to obtain n_1 and n_2. The results are

$$\left.\begin{aligned} Nn_1 &= .105 \pm .010 \\ Nn_2 &= .051 \pm .015, \end{aligned}\right\} \tag{70}$$

in good agreement with (62).

It is natural to ask whether or not the surprisingly large number of singly charged ions is due to residual gas atoms being ionized by either the electrons or by collisions with the recoil atoms. This question can be answered definitely by following the curve in Fig. 21 down to low V values. According to the theory of the instrument, the curve should then proceed as shown by curve A if no singly charged atoms of energy greater than 4 eV existed, whereas the actual fit is obtained, according to section 1.4, with

$$Nn_1 = .100 \pm .010 \tag{71}$$

and independent of the above energy determination

$$T_R = 10 \pm 1 \text{ eV}. \tag{72}$$

It is thus definitely shown that the singly charged ions have the correct energy corresponding to the neutrino emission. Also the pressure extrapolation clearly excludes the above mentioned possibility, as illustrated in Fig. 22. Note that $\langle z_\gamma\rangle$ is determined from

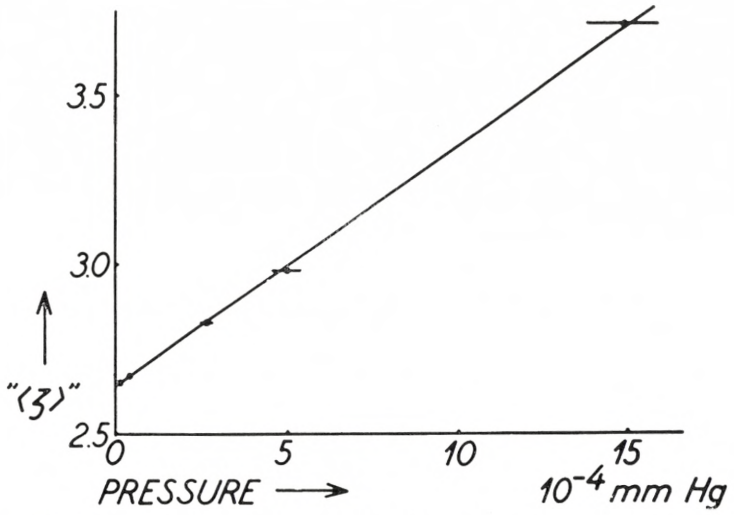

Fig. 22. The calculated $\langle z_{\gamma} \rangle$ value as a function of pressure obtained by calculating from curves not corrected for pressure effects.

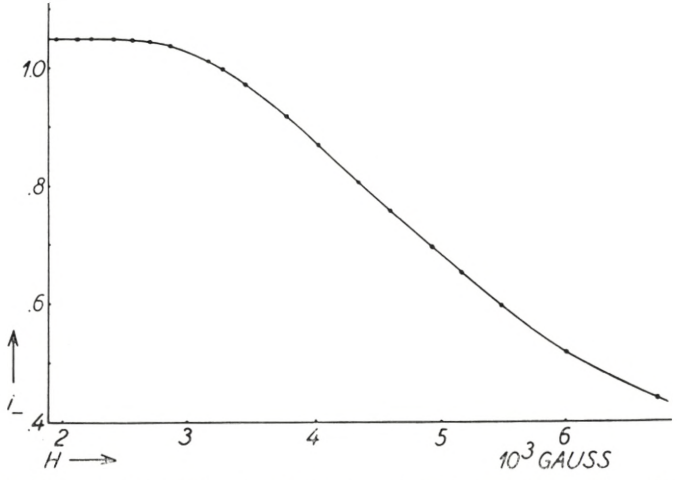

Fig. 23. The recoil contribution to $i_{\_}$ as a function of H for $V = 30$ volts.

(50) and (51) of ref. 2 by inserting $\langle T_R \rangle = 9.6$ eV, implying that we are dealing with high energy ions. This figure gives the results for $\langle z_\gamma \rangle$ which are calculated in this way by interpreting curves like Fig. 17 and Fig. 21, obtained at various pressures.

The average charge does not vary drastically with pressure and the pressure effect consists mainly of a current to the negative plate of ionized gas molecules of low initial velocity.

Finally, the picture so obtained is checked in Fig. 23, which shows an $i_-(H)$ curve for $V = 30$ volts extending into the region where also doubly and singly charged ions can miss the collector. The full-drawn curve represents (61) and (70).

The errors given in the different magnitudes derived in the present section are of course not independent of each other. Presumably the statistics of the data would permit narrowing the limits of errors. However, it is not felt that the sources of systematic errors, especially the effects of the field inhomogeneities, justify a long and involved mathematical treatment of the material (cf. also Appendix B).

3.5. The Secondary Electrons.

Since $Ne\langle z_\gamma \rangle$ is now determined, we can immediately get the average momentum of the electrons from (60). The result is 67 Gauss cm when interpreted directly. However, the small terms in (45) have to be taken into account and thereby we obtain

$$\langle pe \rangle = 69 \pm 1 \text{ Gauss cm.} \tag{73}$$

This value may seem surprisingly low when compared with the generally assumed knowledge about Auger probabilities, Auger energies, and also with the results for the A^{37} decay mentioned in section 3.1. From such considerations it seems natural to have ~ 85 pct of the decays accompanied by 166 Gauss cm Auger electrons from the first Auger effect following K-capture. The average momentum for the remainder of the electrons would accordingly be 16 Gauss cm, corresponding to about 23 eV, which is unreasonably small.

The solution to this anomaly is found by following the curves in Fig. 17 to higher values of $1/H$. For $V = 30$ volts the result is shown in Fig. 24.

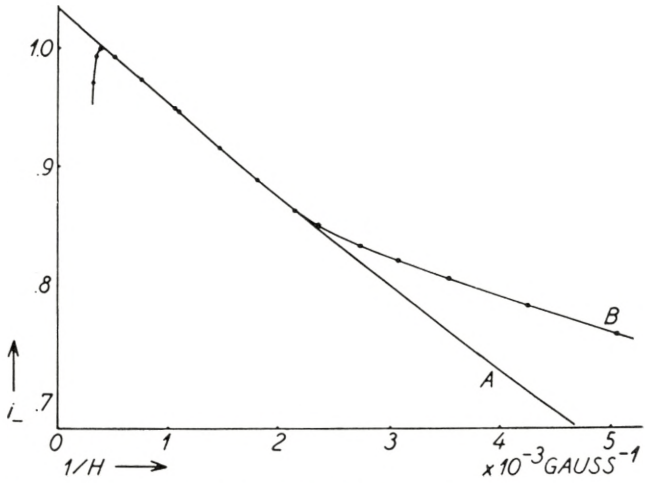

Fig. 24. The same as Fig. 17, but extended to higher l/H values. Curve A is the expected continuation if no electrons of momentum larger than 80 Gauss cm existed. Curve B shows the measurements.

If no electrons of momentum larger than 80 Gauss existed, the points would have to follow the slightly curved line A. The curvature originates from the second term in (45). An analysis of the result according to the picture given in section 1.5 gives the following results:

$$P_{\text{Auger}_I} = 162 \pm 4 \text{ Gauss cm}, \tag{74}$$

corresponding to

$$T_{\text{Auger}_I} = 2320 \pm 120 \text{ eV} \tag{75}$$

and that the intensity of these Auger transitions is

$$N_{\text{Auger}_{I/N}} = 65 \pm 5 \text{ pct.} \tag{76}$$

Correspondingly, the average momentum of the remaining electrons is 32 Gauss cm, corresponding to an energy of 90 eV, which is much more reasonable than the above value, since at least some L–M Auger electrons of energy about 200 eV have to appear[1].

[1] A more detailed analysis of the ionization phenomenon accompanying A^{37} K-capture will be given by A. WINTHER.

3.6. Measurements in Pure Magnetic Fields.

When pure magnetic fields are applied, an especially large pressure correction is expected (cf. section 1.6).

The experimental results obtained in this case are illustrated

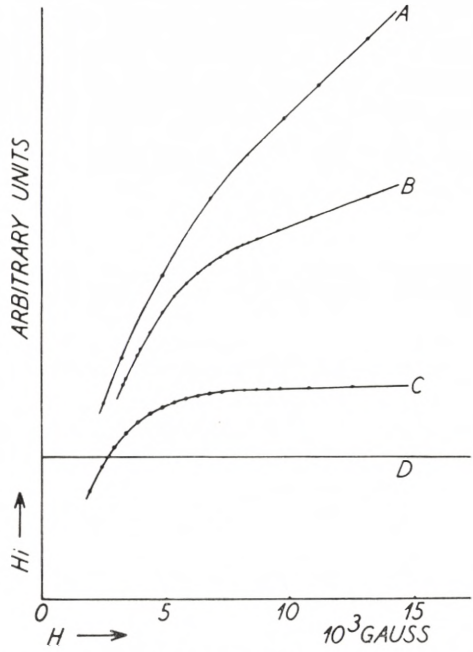

Fig. 25. The figure shows $i(H)$ for $V = 0$. Curve A corresponds to $2 \cdot 10^{-3}$ mm Hg, curve B to $7 \cdot 10^{-4}$ mm Hg, curve C to 10^{-4} mm Hg, and curve D represents the asymptotic behaviour expected from the results in the preceding sections. The currents are given in arbitrary units.

in Fig. 25. Curves are given at various pressures. As expected, the pressure effect is considerably more drastic in these experiments than in the crossed field experiments.

Nevertheless, the points in the 10^{-4} mm Hg curve, where the deviation from the horizontal line occurs, give a good measure of the momentum of the recoils. The determination of Muc gives

$$Muc = 806 \pm 8 \text{ keV}, \tag{77}$$

in agreement with the results measured in crossed fields.

This investigation was actually carried out before the experiments described so far had been performed. The result (77) therefore provided a tool for entering into the analysis of the curve in Fig. 20.

The present curves are of course more uncertain than the curves obtained previously, especially because so high magnetic fields had to be applied that the temperature effect becomes more serious.

Conclusions.

The present investigation gives information about the neutrino recoil momentum in the K-capture of A^{37}. The result is

$$\langle Muc \rangle = 812 \pm 8 \text{ keV}, \tag{78}$$

in agreement with the expectations from the $Cl\ (p, n)\ A^{37}$ threshold of 816 ± 4 keV.

The result (78) has been checked by measuring in pure magnetic fields, "pure" electric fields (72), and crossed electric and magnetic fields.

The charge spectrum is found to be

$$\begin{aligned} n_1 &= 26 \pm 3 \text{ pct.} \\ n_2 &= 13 \pm 4 \text{ pct.} \\ n_3 &= 38 \pm 4 \text{ pct.} \\ n_4 &= 18 \pm 2 \text{ pct.} \\ n_5 &= 4 \pm 1 \text{ pct.} \\ n_6 &= 1 \pm 1 \text{ pct.} \end{aligned}$$

It is ensured that we are dealing with particles of mass ≈ 37 amu. This is due to the fact that really ze/M is measured. We have, furthermore, verified that the charge distribution belongs to particles having the energy corresponding to the neutrino emission.

The average charge of the charged particles is found to be

$$\langle z_7 \rangle = 2.64 \pm .08,$$

which is lower than the values reported previously[6].

Furthermore, the electrons emitted under the charging of the recoils have been investigated, and it is found that Auger electrons are emitted with an energy of

$$T_{\text{Auger}_I} = 2320 \pm 120 \text{ eV}$$

and the relative intensity per disintegration of these electrons is found to be

$$N_{\text{Auger}_I}/N = 65 \pm 5 \text{ pct.} \tag{82}$$

The average momentum of all the electrons is found to be

$$\langle p \rangle = 69 \pm 1 \text{ Gauss cm.}$$

The total information obtained shows a certain degree of internal consistency, and all currents observed have been accounted for.

The results disagree with previous measurements of $\langle z_\gamma \rangle$ and with previous ideas about the ratio of L to K capture and Auger transition probabilities. These two discrepancies are explained if a rather large fraction of all transitions occurs so that an A^{37} K electron is absorbed but where the resultant Cl^{37} atom, due to the radial correlation between the electrons, appears to have a hole in the L shell only[7].

The main source of errors is due to the lack of inhomogeneity of the magnetic field, and a considerably improved instrument could be constructed with the experience gained in our investigations. Many interesting problems could then be attacked and high precision in the important investigations of angular correlation in β-decay could be obtained.

Appendix A.

The functions f, g, and h are defined by means of eqs. (37—39) inside the regions I, II, and III of the A, B plane in Fig. 26. Inside the regions IV and V only a few approximate investigations of the functions have been performed.

The functions have been calculated numerically in regions I,

II and III in the following way. First, tables of the limiting angles (35) and (36) have been computed for suitable values of A' and B. Then, the integrands in (37) and (38) have been calculated, apart from the factor $\sin\theta$, as functions of A' and B. The results of these calculations have, for fixed values of $B = 0$,

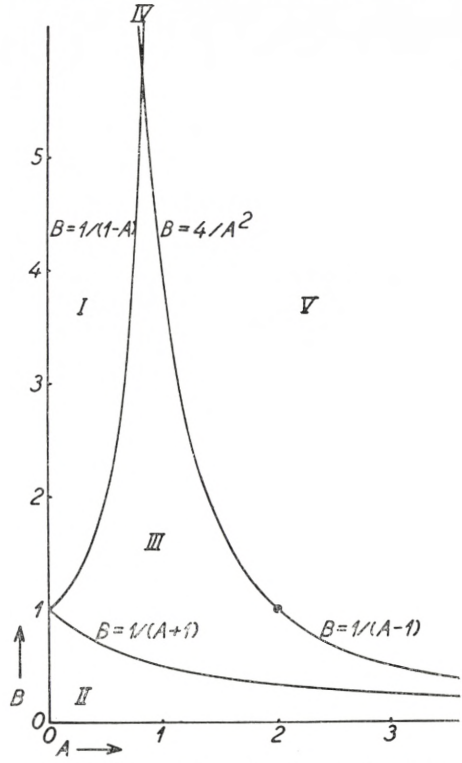

Fig. 26. The regions in the A, B plane.

0.1, 0.2, ... 3.5, been expressed as curves with A' as abscissa. Then, A values = 0, 0.1, 0.2, ... have been chosen and tables of $A \sin\theta$ have been constructed for $\theta = 0°$, $5°$, $10°$ ..... $90°$. The integrands have then been found for these values of A' and multiplied with $\sin\theta$; they have been summed according to Simpson's rule. The functions h and g have thus been obtained with sufficient accuracy for the present investigations, but the accuracy is hardly sufficient when an improved instrument is constructed. The work involved in improved numerical calculations is, however, so great that electronic computers have to be applied.

TABLE 1. $f(A, B) \cdot 1000$.

A	0.0	0.1	0.2	0.3	0.4	0.5	0.6	0.7	0.8	0.9	1.0	1.1	1.2
B													
0.0	000	000	000	000	000	000	000	000	000	000	000	000	000
0.1	100	100	100	101	101	102	103	104	106	107	109	111	114
0.2	200	200	201	202	203	204	206	208	211	214	218	222	227
0.3	300	300	301	302	304	306	309	313	317	321	327	333	340
0.4	400	400	401	403	405	408	412	417	422	428	436	444	454
0.5	500	500	502	504	507	511	515	521	528	536	545	549	
0.6	600	601	602	605	608	613	618	625	629	631	631	627	
0.7	700	701	702	705	710	711	710	708	704	698	691	682	
0.8	800	801	803	805	801	790	778	767	755	743	731	719	
0.9	900	901	893	879	861	842	825	808	791	776	761	747	
1.0	1000	974	951	927	903	881	859	840	820	801	783		
1.1	1000	999	981	961	935	911	887	862	842	820	800		
1.2	1000	1000	996	980	957	931	907	882	858	835	812		
1.3	1000	1000	998	991	970	946	922	897	871	845	820		
1.4	1000	999	998	994	981	959	934	908	881	854			
1.5	1000	999	998	994	986	968	943	917	889	861			
1.6	1000	999	997	994	989	973	950	925	896	867			
1.7	1000	999	997	994	989	976	956	930	901	871			
1.8	1000	999	997	993	988	978	959	933	904	874			
1.9	1000	999	997	993	987	979	962	936	907	876			
2.0	1000	999	997	993	987	979	964	938	909	877			
2.1	1000	999	997	992	986	978	965	939	911	878			
2.2	1000	999	996	992	985	977	965	941	911	878			
2.3	1000	999	996	991	985	976	964	941	911	878			
2.4	1000	999	996	991	984	975	963	941	912	877			
2.5	1000	999	996	991	983	974	961	942	912	877			
2.6	1000	999	996	990	983	973	960	941	913				
2.7	1000	999	996	990	983	973	960	941	913				
2.8	1000	999	995	990	981	971	957	940					
2.9	1000	999	995	989	981	969	956	938					
3.0	1000	999	995	989	980	968	954	936					
3.1	1000	999	995	988	979	967	953	935					
3.2	1000	999	995	988	978	966	951	933					
3.3	1000	999	995	988	878	965	950	931					
3.4	1000	999	994	987	977	964	948	929					
3.5	1000	998	994	987	976	963	946	927					

TABLE 2. $h(A, B) \cdot 1000$.

A	0.0	0.1	0.2	0.3	0.4	0.5	0.6	0.7	0.8	0.9	1.0	1.1	1.2
B													
0.0	000	000	000	000	000	000	000	000	000	000	000	000	000
0.1	0	0	0	1	1	2	3	4	6	7	9	11	14
0.2	0	0	1	2	3	4	6	8	11	14	18	22	27
0.3	0	0	1	2	4	6	9	13	17	21	27	33	40
0.4	0	0	1	3	5	8	12	17	22	28	36	44	54
0.5	0	0	2	4	7	11	15	21	28	36	45	55	66
0.6	0	1	2	5	8	13	18	25	33	41	51	61	
0.7	0	1	2	5	9	15	21	27	35	45	55	66	
0.8	0	1	3	6	10	15	22	28	38	48	60	71	
0.9	0	1	3	6	10	16	22	29	39	51	63	76	
1.0	0	1	3	6	10	16	23	30	40	53	66		
1.1	0	1	2	6	10	16	23	31	42	55	70		
1.2	0	1	2	6	10	16	23	32	43	57	73		
1.3	0	1	2	5	10	17	24	33	45	60	77		
1.4	0	1	2	6	10	17	25	34	47	62	80		
1.5	0	1	3	6	10	18	26	35	48	65	83		
1.6	0	1	3	6	11	18	26	36	50	67	87		
1.7	0	1	3	6	11	19	27	38	52	70			
1.8	0	1	3	7	12	19	28	40	55	72			
1.9	0	1	3	7	13	20	29	42	57	75			
2.0	0	1	3	8	13	21	31	44	60	79			
2.1	0	1	4	8	14	22	32	46	62	81			
2.2	0	1	4	8	15	23	34	48	64	85			
2.3	0	1	4	9	16	24	35	49	68	88			
2.4	0	1	4	9	16	25	37	51	69	92			
2.5	0	1	4	9	17	26	38	53	72	96			
2.6	0	1	4	10	18	27	40	55	73	98			
2.7	0	1	5	10	18	29	41	56	76	104			
2.8	0	1	5	11	19	30	43	59	78				
2.9	0	1	5	11	20	31	44	61					
3.0	0	1	5	11	20	32	46	63					
3.1	0	1	5	12	21	33	47	65					
3.2	0	1	5	12	22	34	49	67					
3.3	0	1	6	12	22	35	51	69					
3.4	0	1	6	13	23	36	52	71					
3.5	0	2	6	13	24	37	54	73					

As long as the deviation from the $A = 0$ case treated in section 1.2 is small, we are, nevertheless, justified in applying the present procedure. Finally, the function f is obtained from formula (39).

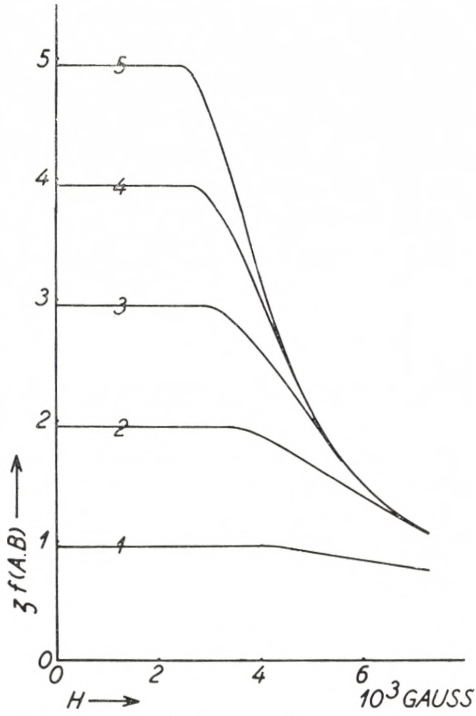

Fig. 27. The current $i_{\_}$ resulting from particles of different charges, $Muc = 812$ keV, $H = 37$ amu, and $V = 30$ volts and $a = .352$ cm as a function of H.

Inside areas I and II the functions are especially simple. Inside area I we have

$$j_I(A, B) = 0 \tag{84}$$

and

$$h_I(A, B) = B \int_0^{\pi/2} \frac{1}{2\pi} \sin\theta\,(1 + A')E(k, \pi/2)/\theta = B\,S(A). \tag{85}$$

Inside area II one finds

$$j_{II}(A, B) = 1 - B - 4\,B\,S(A) \tag{86}$$

and

$$h_{II}(A, B) = 2\,B\,S(A). \tag{87}$$

The function $S(A)$ is, for small values of A, given by

$$S(A) \simeq \frac{A^2}{24} + \frac{A^4}{480} + \frac{A^6}{2240} + \frac{5\,A^3}{32256}. \tag{88}$$

The results for the functions f and h are illustrated in Tables 1—2.

By means of the functions f, g, and h one can find the currents belonging to a given charge distribution, say, for a given value of V and as functions of H. This is illustrated in Fig. 27.

Appendix B.

The data obtained in the present investigation are not well suited for a least square fit. The number of decimals needed in handling the mathematics sufficiently precisely is tremendous. This is perhaps best illustrated by a simple example. Suppose that measurements were performed, leading to a set of equations of the type (22). Say, for simplicity,

$$\left.\begin{aligned} n_1 + \quad n_2 + \quad n_3 &= 100.1 \\ n_1 + 2\,n_2 + 2\,n_3 &= 175.0 \\ n_1 + 2\,n_2 + 3\,n_3 &= 199.9 \end{aligned}\right\} \tag{89}$$

corresponding to $n_1 = 25$, $n_2 = 50$, and $n_3 = 25$ and an accuracy of .1. Now use the method of least squares. Thereby, one finds

$$\left.\begin{aligned} n_1 + 1.667\,n_2 + 2.000\,n_3 &= 158.33 \\ n_1 + 1.800\,n_2 + 2.200\,n_3 &= 169.98 \\ n_1 + 1.833\,n_3 + 2.333\,n_3 &= 174.96 \end{aligned}\right\} \tag{90}$$

which are nearly linearly dependent and need an even larger number of digets than given in order to yield as accurate results as (89).

Appendix C.

The selection of insulator material was made by testing the properties of different insulators by means of the vibrating reed electrometer. We shall describe the results with textolite only because this material was actually used in the instrument. A test

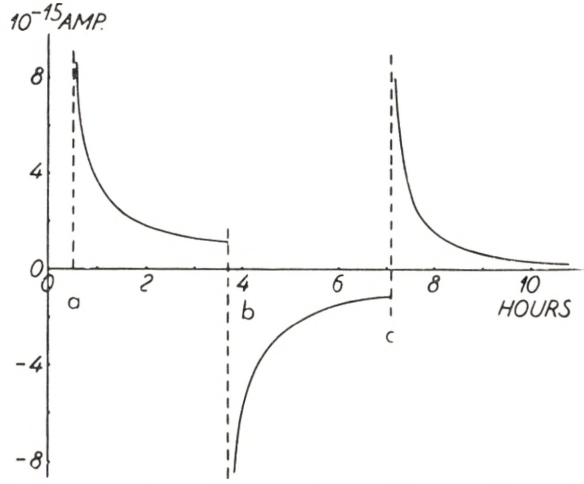

Fig. 28. Currents through textolite insulator as a function of time when a voltage of 120 volts is applied across the insulator. At $t = a$ the voltage is switched on, at $t = b$ the voltage is reversed in sign, and at $t = c$ the voltage is switched off.

body was inserted between two condenser plates, one of which was connected to the electrometer. An extra condenser plate provided the tool for connecting a dry cell across the test body in such a manner that possible drift in the dry cell voltage was eliminated according to the scheme given in Fig. 10 of section 2.3. The test chamber was evacuated in order to eliminate cosmic ray ionization.

When the voltage is switched on, currents occur due to the residual components of the dielectric polarization. This is of course important for the recoil spectrometer also. It means that all insulators which can be seen by the insulated system connected to the vibrating reed have to be left undisturbed as regards electric potential changes for sufficiently long time before measurements can start. The effect is illustrated in Fig. 28.

In our case, the insulators are subjected to heavy irradiations. It is quite reasonable to represent the three insulators K in Fig. 7 of section 2.2 by one textolite resistance of $1/\sigma$ ohms, where σ is the specific conductivity in $\text{ohm}^{-1}\ \text{cm}^{-1}$. This insulator is placed in a radiation field, but it is fairly well protected by the condenser plate II. Thus we get an overestimate by considering 1 cm³ textolite placed in the full radiation field. Since we are attempting an approach to an infinitely extended system, the radiation intensity will be given by[8)]

$$I = 3.7 \times 10^7\, n \times \frac{T}{30} \cdot 4.8 \cdot 10^{-10}\, 3600 \text{ rep/hour}, \qquad (91)$$

where n is the concentration of radioactivity in millicuries per cm³ and T is the transition energy minus the neutrino energy in eV.

Thus, the conductivity at time t, measured in hours after the gas inlet, will be given by[9)]

$$\left.\begin{aligned} \sigma_1 &= g I^h \tanh^\alpha (b g I^h t) \\ &\simeq g I^{1/2} \tanh^\alpha (I^{1/2}\, t/25) \to g I^{1/2}, \end{aligned}\right\} \qquad (92)$$

where g, h, α, b are constants characteristic of the material. The approximation made is sufficient for our purpose because we are especially interested in g and the ultimate value of σ_1, after a long irradiation. The above mentioned test body was subjected to an irradiation of 250 röntgens per hour for 20 hours so that the ultimate value of σ_1 was obtained. The measurements of σ carried out after termination of the irradiation follow a curve of the form[9)]

$$\sigma = \frac{1}{1/\sigma_1 + kt}, \qquad (95)$$

where t is measured from the termination of the irradiation, and k is another constant characteristic of the material. From the experimental result, σ_1 is found to be $10^{-16.7}$ and, consequently, one obtains $g = 10^{-17.9}$.

For A^{37} we have $T \approx 3000$ eV, and we are using $u = 10^{-3}$ millicurie per cm³. Thus we get $I = 6.4$ röntgen per hour, which leads to $\sigma_1 = 10^{-17.5}$, which is quite satisfactory.

Aknowledgements.

The authors wish to express their sincere gratitude to professor NIELS BOHR for his interest in our experiments and for the facilities placed at our disposal. We also wish to thank Civ. ing. H. TUXEN MEYER for designing the magnet.

Institute for Theoretical Physics,
University of Copenhagen,
Denmark.

References.

1) J. C. JACOBSEN and O. KOFOED-HANSEN, Phys. Rev. **73**, 675 (1948), O. KOFOED-HANSEN and P. KRISTENSEN, Dan. Mat. Fys. Medd. **26**, no. 6 (1951).
2) O. KOFOED-HANSEN, Dan. Mat. Fys. Medd. **26**, no. 8 (1951).
3) J. R. JENSEN and K. O. NIELSEN, Ingeniøren, Nr. 23 (1952).
4) For references, see J. M. HOLLANDER, I. PERLMAN, and G. T. SEABORG, Rev. Mod. Phys. **25**, 469 (1953).
5) G. W. RODEBACK and J. S. ALLEN, Phys. Rev. **83**, 215 (1951).
6) M. S. PERLMAN and J. A. MISKEL, Phys. Rev. **91**, 899 (1953). S. WEXLER, Phys. Rev. **93**, 182 (1954).
7) P. BENOIST-GUEUTAL, thesis, Paris (1953).
8) L. H. GRAY, Proc. Roy. Soc. **A 122**, 648 (1928). O. KOFOED-HANSEN, Arkiv för Fysik **2**, 216 (1950).
9) D. K. KELL, S. KAGANOFF, C. H. MAYHEW, and H. G. NORDLIN, NYO-4518 (1953).

Indleveret til selskabet den 7. januar 1955.
Færdig fra trykkeriet den 8. september 1955.